Chinese Chemical Letters 34 (2023) 107478

Contents lists available at ScienceDirect

Chinese Chemical Letters

journal homepage: www.elsevier.com/locate/cclet

The fabrication strategies and enhanced performances of metal-organic frameworks and carbon dots composites: State of the art review

Yanqiu Zhang[a], Minrui Sun[a], Mingguo Peng[a,*], Erdeng Du[a], Xia Xu[a], Chong-Chen Wang[b,*]

[a] School of Environmental and Safety Engineering, Changzhou University, Changzhou 213164, China
[b] Beijing Key Laboratory of Functional Materials for Building Structure and Environment Remediation/Beijing Energy Conservation & Sustainable Urban and Rural Development Provincial and Ministry Co-construction Collaboration Innovation Center, Beijing University of Civil Engineering and Architecture, Beijing 100044, China

ARTICLE INFO

Article history:
Received 17 February 2022
Revised 16 April 2022
Accepted 28 April 2022
Available online 1 May 2022

Keywords:
Carbons dots
Metal-organic frameworks
Synthesis
Photocatalysis
Sensors

ABSTRACT

Metal-organic frameworks (MOFs) with large specific surface area, considerable pore volume, controllable structure, and high concentration of active metal sites have been applied widely in researches like catalysis and sensing. However, potential applications of MOFs in both photocatalysis and luminescence sensors are facing major challenges arising from their severe charge recombination, low utilization of solar energy, low quantum yield, limited charge transfer between the metal ions/clusters and the ligand. Recent studies revealed that rational introduction of carbon dots (CDs) with excellent optical properties, unique quantum confinement and high conductivity can greatly enhance the functions of MOFs. In this paper, typical synthesis methods of these CD-MOF composites as well as their potential applications in photocatalysis and sensing are reviewed with emphasis. Representative examples of these CD-MOF composites are discussed, and key features and advantages of CD-MOF composites that will facilitate future applications are highlighted.

1. Introduction

Metal-organic frameworks (MOFs) with infinite framework structures are assembled with metal centers/clusters and organic linkers, offering unique chemical properties with exceptional large and permanent micropore. The varied chemical compositions make MOFs designable in both structure and performance, thus making applications possible in catalysis [1–6], adsorption [7–10], separation [11–13], gas storage [14–16], sensors [17–22] and drug delivery [23–25]. But MOFs have some deficiencies like severe charge recombination as photocatalysts and low quantum yield (QY) as luminescence sensors. Therefore, MOFs-based composites, combining the excellent properties of MOFs and guest materials, have been designed to rid the shortcomings of the instinct MOFs.

Yaghi and his co-workers reported for the first time a series of novel host-guest framework composites by introducing fullerenes and other organic dyes into a new MOF named MOF-177 [26]. Since then, increasing investigations have focused on adopting MOFs as unique host matrices to construct new composites with the secondary materials. Up to now, secondary materials including metal/metal oxides [27–29], carbon nanotubes [30–32], quantum dots [33,34] and polymeric molecules [35] have already been introduced to combine with MOFs to improve their performance in applications like catalysis, gas-storage, and sensing [36–39].

Carbon dots (CDs), as new class of luminescent nanoparticles with the size of quantum including graphene quantum dots (GQDs), amorphous carbon nanoparticles and polymer dots (PDs) [40,41], have attracted interest due to their properties like unique optical properties, physicochemical stability, low toxicity, environmental friendliness and excellent biocompatibility. Additionally, the optical properties of CDs can be adjusted by doping with other elements or controlling condensation reaction and chemical manipulations. The most commonly used element is nitrogen (N), and other elements such as boron (B) and sulfur (S) are usually doped with a combination of nitrogen. Despite the above advantages, high concentrations of CDs usually result in aggregation and collision, which in turn induces emission quenching. However, numerous studies suggest that encapsulation of CDs in porous materials is an effective way to solve these problem [42–44]. It is worth noting

* Corresponding authors.
E-mail addresses: pmg@cczu.edu.cn (M. Peng), wangchongchen@bucea.edu.cn, chongchenwang@126.com (C.-C. Wang).

https://doi.org/10.1016/j.cclet.2022.04.076
1001-8417/

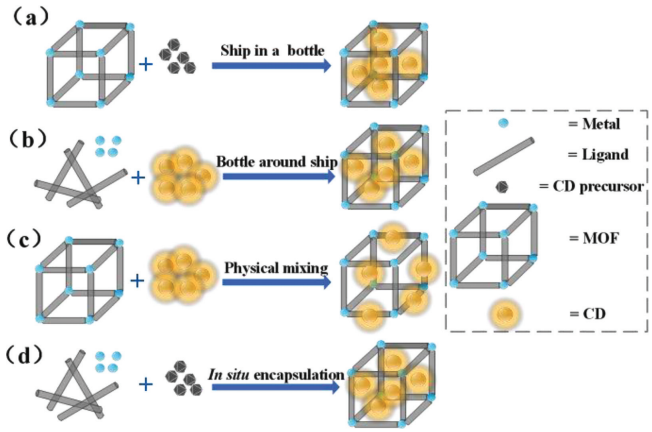

Fig. 1. Strategies for CD-MOF composites construction. (a) "Ship in a bottle". (b) "Bottle around ship". (c) "Physical mixing". (d) *In situ* encapsulation.

that MOFs exhibit extremely high porosity and have an adjustable pore size, making them ideal substrates for CDs' combination.

Hence, gradually there are studies on constructing composites using different MOFs as host materials and CDs as guest ones (hybrids denoted as CD-MOF). Recently, progresses have been made in the construction and application of CD-MOF composites. Especially, the integration of the merits of MOFs and CDs produces many excellent properties which are superior to those of individuals as follows. (i) Taking the advantage of CDs and/or MOFs luminescent emission in high quantum yield, a large number of CDs-MOFs are found to be photoluminescent. Coupled with host MOFs with ultrahigh porosities and surface areas, CD-MOF composites can act as fluorescent sensing platforms with high sensitivity and selectivity for analytes [42]. (ii) Most MOFs manifest insulating properties, while the development of CD-MOF improves their conductivity [45]. (iii) The tight interface and band gap matching between CDs and MOFs can accelerate the separation of photogenerated charges and inhibit the recombination of photogenerated electrons and holes effectively, and further enhance the photocatalytic performance.

A review paper concerning the applications of CD-MOF composites as sensors has been published [42], but no comprehensive coverage of other applications is provided. Thus, it is necessary to make a clear classification of potential applications of CD-MOF, figure out the properties of CD-MOF composites, and identify the roles of CD or MOF in their composites for various potential applications. This review aims to present the state-of-the-art advances in CD-MOF composites, in which the fabrication strategies, structural characteristics and applications are highlighted. And, future development trend in this field is discussed. We expect that the information in this paper can serve as a basis and guidance for the rational design and research of CD-MOF composites.

2. Preparation of CD-MOF composites

Various CD-MOF composites with multiple properties (catalysis, fluorescence, *etc*) have been prepared with different construction strategies. Based on the previous reports, three well established routes are demonstrated in Fig. 1. The first strategy involves a "ship in a bottle" synthetic process by mixing initial precursors of CD in the pre-synthesized MOF, and further being treated with calcination or other methods to transform precursors of CD into the desired CD (Fig. 1a). This method might limit the growth and alignment of CD, but avoid the agglomeration of CD by immobilizing CD in MOF cavities. The second strategy called "bottle around ship" involves the pre-preparation of CD and the assembling of MOF precursors around CD (Fig. 1b). Similar with "ship in a bottle", CD can be encapsulated in the matrix of MOFs and the agglomeration of CD can be avoided with this method. More importantly, since CD can be pre-prepared, the size and shape of CD can be adjusted for application. For example, "bottle around ship" is the most used method for the construction of CD-MOF based fluorescent sensors, which enabled CD with fluorescence pre-adjusted for the sensing target. The third strategy "Physical mixing" comprises a process to construct CD-MOF composites by directly mixing the pre-synthesized CD and MOF, which combined CD and MOF by adsorption or binding with the aid of some agents (Fig. 1c). In this method, CD tends to be immobilized on the surface of MOF, in which both the structure and properties of CD and MOF can be retained and more targeted for applications. Besides the three well established methods, other novel and feasible methods were also reported, such as "*In situ* encapsulation" (Fig. 1d), "calcination" and "electrodeposition".

2.1. Ship in a bottle

With "ship in a bottle" method, MOF matrix was prepared first and then CDs was synthesized in the MOF under certain conditions.

For example, Li *et al.* embedded CQDs in MIL-53(Fe) adopting "ship in a bottle" method (Fig. 2a) [46]. They prepared and activated MIL-53(Fe) with well-defined pore channels as template, and infiltrated glucose molecules in ethanol and deionized water for 24 h. After heating to remove the solvents and washing to remove glucose molecules on MOF surface, the obtained powders were calcined under 200 °C to obtain the final product MIL-53(Fe)/CQDs. In this process, the high inner pore surface area of MIL-53(Fe) and the adequate washing prior calcination ensured that the CQDs were formed in the pores of MIL-53(Fe). Although no obvious morphology change was found in SEM or TEM images after the introduction of CQDs in MIL-53(Fe) (Figs. 2b-e), CQDs can be observed in TEM images after dissolving MIL-53(Fe) in KOH solution (Fig. 2f), affirming the encapsulation of CDs in the pore of MIL-53(Cr). Same method was used to fabricate a heterogeneous nanocatalyst in Gholami's work [47]. A Fe-based MOF (MIL-88B(Fe)) was synthesized from $FeCl_3{\cdot}6H_2O$ and terephthalic by the solvothermal method firstly, and then it was dispersed into the glucose solution and stirred for 7 h. After being washed and dried, the collected products were calcined under 200 °C for 2 h to obtain CDs/MIL-88B(Fe). In this work, Bi_2S_3 nanoparticles were further decorated on CDs/MIL-88B(Fe) with "ship in a bottle" method and obtained the final product CDs/MIL-88B(Fe)/Bi_2S_3.

Another ternary composite was prepared with "ship in a bottle" method by introducing both CDs and CdS into MIL-101 pores according to the process in Fig. 2g [48]. MIL-101 was firstly prepared with $Cr(NO_3)_3{\cdot}9H_2O$ and terephthalic acid by a typical synthesis process and suspended in *n*-hexane solvent with 2 h stirring. Then $Cd(Ac)_2$ glucose aqueous solution and Na_2S glucose solution were respectively dropped in the above solution with constantly stirring. After being continuously stirred for 12 h, green powder was obtained *via* filtration. CDs were formed with dried green powder for 12 h under 80 °C and calcined 2 h at 200 °C under N_2 atmosphere. With further being heated at 180 °C and 80 °C for 12 h and 6 h under vacuum condition, the targeted CD/Cds@MIL-101 was obtained. In addition, ultra-small CDs were found to be incorporated into the pores of CD/Cds@MIL-101, which was affirmed by both TEM and HRTEM observations (Figs. 2h-k).

Based on the above descriptions, CD-MOF composites synthesized with the "ship in a bottle" method can accomplish the encapsulation of CD in the pores of MOF, which can inhibit the agglomeration of CDs to achieve CD-MOF composite with outstanding performance in catalysis, sensing and other applications. But

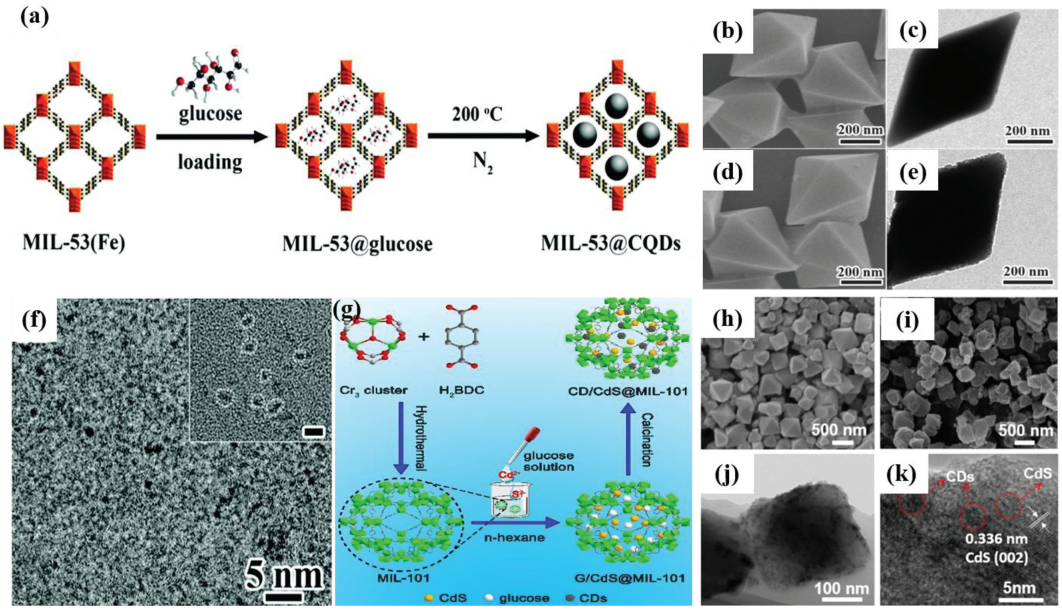

Fig. 2. (a) Synthetic process of MIL-53@CQDs. SEM and TEM images of MIL-53(Fe) (b, c) and MIL-53(Fe)/CQDs (d, e). (f) TEM image of CQDs after dissolving MIL-53(Fe) with KOH (1 mol/L). (a-f) Copied with permission [46]. Copyright 2018, the Royal Society of Chemistry. (g) Synthetic process of CD/CdS@MIL-101. TEM and HRTEM images of MIL-101 (h, j) and CD/CdS@MIL-101 (i, k). (g-k) Copied with permission [48]. Copyright 2019, Elsevier.

high-temperature calcination or long-time immersion are usually needed in this method, thus requiring high water/thermal stability of MOF materials.

2.2. Bottle around ship

The "bottle around ship", known as template synthesis method, involves the pre-synthesized CDs and initial precursors of MOFs. In this method, CDs are firstly synthesized and usually dispersed in solvent and stabilized with capping agents or surfactants. Then, MOF precursors (metals, ligands) are added the solvent to construct MOF incorporated with CDs.

In 2014, Lin *et al.* reported the encapsulation of branched poly(ethyleimine)-capped CQDs (BPEI-CQDs) into ZIF-8 with "bottle around ship" method [44]. BPEI-CQDs was firstly prepared and then added in the solution of 2-methylimidazole and $Zn(NO)_2{\cdot}6H_2O$ for 24 h at room temperature. The as-synthesized BPEI-CQDs/ZIF-8 remains the crystalline integrity of ZIF-8 and exhibits strong blue fluorescence under 365 nm UV-light ascribed to BPEI-CQDs. In 2016, Xu *et al.* obtained CDs@ZIF-8 by preparing CDs with the facile hydrothermal method and mixed it with zinc nitrate aqueous solution and 2-methylimidazole [49]. Similar with BPEI-CQDs/ZIF-8, CDs@ZIF-8 remained the crystal structure of ZIF-8 and obtained the fluorescence property of CDs.

Based on above work, two-emission luminescent composites were prepared and usually used as ratiometric sensors, in which CD-MOF composites were synthesized with "bottle around ship" and another fluorescent signal subsequently introduced. Gao *et al.* constructed a ratiometric sensor for hydrogen sulfide (H_2S) sensing [50]. They firstly prepared CDs@ZIF-8 with "bottle around ship" method similar to Xu's work [49], and further fabricated CDs@ZIF-8@GMP/Tb with CDs@ZIF-8, GMP and Tb^{3+} as precursors spontaneously. In CDs@ZIF-8@GMP/Tb composites, CDs was encapsulated in ZIF-8 with the integrity of ZIF-8 maintained, and GMP/Tb formed a film coated on CDs@ZIF-8 to produce the interaction between Tb^{3+}, phosphate and nucleobase moieties. Weng *et al.* constructed a two-emission luminescent composite N-GQDs/Eu^{3+}@Mg-MOF to sense atmospheric benzene homologues [51]. In this work, N-dropped GQDs (N-GQDs) were firstly prepared with ethylenediamine and citric acid under hydrothermal conditions, and then the N-GQDs were doped into Mg-MOF *via* "bottle around ship" method. Finally, Eu^{3+} was encapsulated in N-GQDs doped Mg-MOF composite by replacing residual $[(NH_3)_2Me_2]^+$ in pores. The obtained N-GQDs/Eu^{3+}@Mg-MOF composites exhibited a dual-emission from N-GQDs and Eu^{3+} under the excitation of 394 nm and another dual-emission of ligand-based emission and Eu^{3+} under the excitation of 349 nm.

Two-emission luminescent composites can also be prepared by directly introducing CD into the fluorescent MOF with "bottle around ship" method. Fu *et al.* prepared CDs@MOF(Eu) composite as a fluorescent sensor by introducing the ethanediamine-modified CDs into MOF(Eu) (precursors: $Eu(NO_3)_3{\cdot}6H_2O$, 1,3,5-benzenetricarboxylic acid) with "bottle around ship" method [52]. CDs@MOF(Eu) composite maintained the structure and rod-like morphology of MOF(Eu) and exhibited a dual-emission of CDs and Eu^{3+}. In 2016, a dual-emission composite (EuMOFs/N,S-CDs) for water molecule detect in organic solvents was fabricated by encapsulating the blue light emitting N/S doped carbon-based dots (N,S-CDs) into the Eu-MOFs with red light emission (precursors: $Eu(NO_3)_3{\cdot}6H_2O$, 1,3,5-benzenetricarboxylic acid) by "bottle around ship" method [53].

With the "bottle around ship" method, agglomeration of CDs on the surface of MOF can be avoided to a great extent and suitable CDs can be pre-prepared for the target application. But the growth of MOFs and the fluorescence of CDs might be influenced in the synthesis process, thus rational choose of MOFs and CDs is vitally in this synthetic method.

2.3. Physical mixing

Another facile synthetic method for CD-MOF is physical mixing. In this method, both CDs and MOFs are pre-synthesized and mixed directly, forming the CD-MOF with the interaction between CD and MOF or the combination with some binding agent. Yang *et al.* reported an amine-CQDs@UiO-66 composite by directly immersing the pre-synthesized UiO-66 in amine-CQDs solution at room temperature for 12 h [54]. In this work, fluorescent amine-CQDs were immobilized in the framework by replacing the coordinated

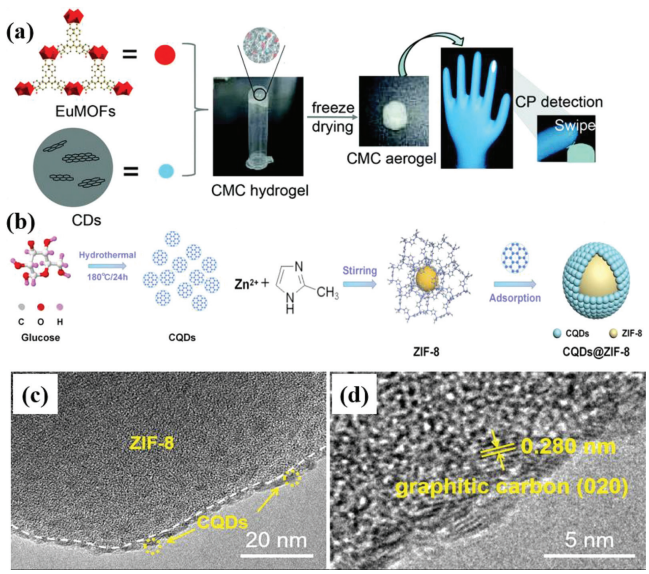

Fig. 3. (a) Construction process of the wearable sensor EuMOFs/CDs@CMC. Copied with permission [56]. Copyright 2018, the Royal Society of Chemistry. (b) Scheme of the preparation process of CQDs@ZIF-8. TEM (c) and HRTEM (d) images of CQDs@ZIF-8. Copied with permission [57]. Copyright 2020, Springer Link.

DMF, entering the channels of UiO-66 and acting as a functional monomer to detect the target molecules.

To accomplish highly selective and sensitive detect the target molecules, Xu *et al.* developed a novel fluorescent sensor based on CDs embedded ZIF-8@molecularly imprinted polymer (MIP) (CDs@ZIF-8@MIP) [55]. They mixed the pre-synthesized CDs and ZIF-8, and added the mixture in the solution with template molecule (quercetin, QCT), functional monomer (4-vinylpyridine, 4-Vp), cross-linker (ethylene glycol dimethacrylate, EGDMA) and initiator (2,2-azobisisobutyronitrile, AIBN) to carry out polymerization. In this sensor, ZIF-8 acted as support with its large surface area and pores, the molecularly imprinted polymer acted as the adsorption and recognition component for the target molecules, and CDs sense the interaction and transduce to fluorescence signals visible to naked eyes. Xu *et al.* directly mixed the dried Eu-MOFs and CDs powder in aqueous solution and combined them with CMC aerogel to fabricate a ratiometric glove sensor (Eu-MOFs/CDs@CMC) (Fig. 3a) [56], in which CMC was used as a host material with powerful adsorption capability. In addition, the assisting mean such as ultrasonic hybridization was also used in physical mixing. For example, Si *et al.* mixed CQDs solution with ZIF-8 suspension and sonicated for 30 min with the aid of ice bath to obtain CQDs@ZIF-8 [57] (Fig. 3b). TEM images in Fig. 3c indicated CQDs@ZIF-8 exhibit a core-shell structure, in which the edges of ZIF-8 are wrapped with CQDs in 3-5 nm sizes. In addition, the wrapped CQDs possess good crystallinity with clear lattice fringes in HETEM image (Fig. 3d).

As the characteristics of both CDs and MOFs can be pre-adjusted, the prepared CD-MOF with physical mixing method can be more facilely targeted for application. With this methodology, the distribution of CD involves diverse forms like adsorbing on the MOF surface and/or occupying the pore space of the framework.

2.4. Other methods

The "*In situ* encapsulation" is the method to construct CD-MOF composites by mixing both precursors of CD and MOF and then reacting at a certain condition. Yao *et al.* fabricated CDs@UiO-66-$(OH)_2$ by a facile solvent-free method, in which CDs were formed *in situ* during the initial stages of UiO-66-$(OH)_2$ [58]. The PXRD patterns validated the successful preparation of UiO-66-$(OH)_2$, and CDs with spherical morphology in 3-8 nm sizes were discovered in high-resolution TEM (HRTEM). In addition, compared to UiO-66$(OH)_2$, the surface area of CDs@UiO-66-$(OH)_2$ decreased, indicating that CDs was successfully encapsulated in UiO-66$(OH)_2$. This method possessed the merits of simple operation and less solvent demand. However, the formation conditions of CDs and MOFs are usually different. From this point, the "*In situ* encapsulated" method should avoid the mutual influence between the CDs and MOFs.

Wang *et al.* prepared CNDs@ZIF-8 composites (CND = carbon nanodots) with "calcination" method [59]. Briefly, they synthesized ZIF-8 with mixing and stirring $Zn(NO_3)_2{\cdot}6H_2O$ and dimethyl imidazole (Hmim) in methanol. Then they calcined ZIF-8 nanoparticles in the oven at 200 °C for certain hours. The CNDs@ZIF-8 was obtained with the framework structure and the shape of ZIF-8 being remained. CNDs appeared in ZIF-8 nanocrystals and showed a 0.21 nm lattice spacing consistently with the (100) plane of graphene in HR-TEM images, which derived from some of the organic ligands (Hmim). Moreover, with the formation of CNDs, some organic ligands were broken to induce the formation of cavities, resulting in a higher surface area of CNDs@ZIF-8 than ZIF-8. Two emission peaks of CNDs@ZIF-8 at 447 nm and 550 nm appeared under the irradiation of 380 nm UV light, which were ascribed to the emission of ZIF-8 and CNDs, respectively.

Hou *et al.* deposited a chiral carbon quantum dots (CCQDs) on the surface of a Cu based MOF (Cu-TDPAT [60]) to fabricate MOF@CCQDs/NiF composites by a three-electrode system [61]. The treated NiF, platinum plate and calomel electrode were adopted as working electrode, counter electrode and reference electrode, respectively. As well, the CCQD suspension and precursors of Cu-MOF was selected as the electrolyte. The characterization results indicated that MOF@CCQDs/NiF maintained the original framework of the host MOF. Electrochemical impedance spectroscopy (EIS) tests demonstrated that electrochemical behavior of the obtained composites was significantly improved by the introduction of CCQDs, which increased the surface area of the electrode and boosted the interactions between electrode surface and negatively charged potassium ferricyanide.

All above mentioned strategies are suitable for CD-MOF composites construction. The main difference lies not only in the synthesis steps, but also in the various forms of CD on MOF in the composite, giving those as-prepared composites different characteristics and properties. For example, the encapsulation of CDs into MOF matrixes can promote the formation of heterojunctions, prevent CDs from agglomeration, accelerate the separation of charges and promote the catalytic performance of CD-MOF composites. Thus, rational configuration of MOF and CD can greatly enhance their performance in different applications.

3. Application for photocatalysis

Although MOFs with porous crystallin structures exhibited unique advantages as photocatalysts [62], their catalytic effects are still limited by quick charge recombination and low utilization of sunlight energy. To rid these limitations, MOFs have been assembled with narrow gap semiconducting materials, such as S-TiO_2 [63], $Bi_{12}O_{17}Cl_2$ [64], polyaniline (PANI) [65], $Cd_{0.5}Zn_{0.5}S$ [66], N-$K_2Ti_4O_9$ [67], $Bi_{24}O_{31}Br_{10}$ [68], titanate nanotube [69], g-C_3N_4 [70] in our previous research work. Similarly, CDs were chosen as cocatalyst for MOFs in recent studies, playing versatile roles as electron receptor, photosensitizer and/or spectral converter in different photocatalytic systems [71]. Here, we summarized the recent CD-MOF composites reported in photocatalysis, which mainly focused on the application of environmental remediation and energy production.

Table 1
CD-MOF composites for environmental remediation.

Photocatalyst	Synthesis method	Applications	Band gap	Light source	Performance	Cycles	Role of CDs	Ref.
MIL-53(Fe)/CQDs	Ship in a bottle	Cr(VI) reduction	2.79 eV	Visible light	Most of the Cr(VI) (8 mg/L $K_2Cr_2O_7$) ions was reduced to Cr(III) in 50 min	-	Electron acceptor, photosensitizer	[46]
N-CQD/MOF-5	Bottle around ship	Cr(VI) reduction	3.41 eV	Visible light	2.5 times than that of pure MOF-5 under 1 h irradiation	5	Electron acceptor	[72]
CQDs/NH_2-MIL-125	Physical mixing	RhB degradation	2.35 eV	Full spectrum Visible light	100% in 120 min 100% in 200 min	7	Electron-acceptor, spectrum converter	[73]
CQDs@ZIF-8	Physical mixing	MB degradation	4.95 eV	Sunlight Visible light	91% 78%	3	Electron acceptor, photosensitizer	[57]
CDs/MIL-88(Fe)/Bi_2S_3	Ship in a bottle	4-Nip reduction	-	-	Reduce all of the 4-Nip to 4-Amp in 240 s	-	Assisting electron relay	[47]
		MB degradation		Visible light	60%	4	Enhance the electron-hole pair separation	
		AB92 degradation		Visible light	75%	4	Enhanced electron-hole pair separation	
GQDs/UiO-66-NH_2/NW-PP	Impregnate a non-woven polypropylene substrate in UiO-66-NH_2 suspension and injected with GQDs	MB degradation	-	Combinatory UV and visible light	98.6%	-	Enhanced electron-hole pair separation	[74]
GQDs/UiO-66-NH_2/ZnO/AISI steel	Impregnation of UiO-66-NH_2 and spray GQD on the ZnO coated AISI 304 steel meshes	Oleic-acid degradation	-	UV light	Degradation of the oleic-acid completely after 9 h	3	Photosensitizer	[75]

3.1. Environmental remediation

CD-MOF composites have received great attentions in environmental remediation applications such as the organic pollutants degradation and Cr(VI) reduction. The latest developments in environmental remediation using CD-MOF composites are discussed below and summarized in Table 1.

Considering the stable topology and photo response properties, MIL-53(Fe) was chosen and further embedded with CQDs inside the pores with "ship in a bottle" method to photocatalytically reduce Cr(VI) into Cr(III) [46]. The preparation process and morphology of MIL-53(Fe)/CQDs are illustrated in Ship in a bottle section. The UV-vis diffuse reflection spectrum (DRS) (Fig. 4a) showed that MIL-53(Fe)/CQD composites possessed a similar absorption behavior as MIL-53(Fe) but wider absorption edges, indicating the photocatalytic performance enhancement in visible region. Moreover, as depicted in the band structure diagram (Fig. 4b), the conduction band minimum (CBM) of MIL-53(Fe)/CQDs is −0.44V, which is more negative than the potential of Cr(VI)/Cr(III) (0.51 V, pH 6.8). According to the thermodynamic perspective, Cr(VI) can be easily reduced to Cr(III) with MIL-53(Fe)/CQDs. As expected, the photocatalytic activity for Cr(VI) reduction was improved with the appearance of CQDs, in which MIL/C-9 (MIL-53(Fe)/CQDs carbonized with 9.0 mg glucose) exhibited best photocatalytic Cr(VI) reduction activity under pH being 4.0 (Fig. 4c). Specifically, overloading of CQDs may result to recombination of photo-induced electron-hole pair and shield of incident light for MIL-53(Fe)/CQDs, thus decreasing the photocatalytic activities. The improved photocurrents (Fig. 4d) and decreased charge transfer resistance (R_{ct}) (Fig. 4e) of MIL-53(Fe)/CQDs indicated the improvement of separation of the photo-induced charge carriers and charge transfer rate after the introduction of CQDs to MIL-53(Fe), which led to the superior photoactivity of MIL-53(Fe)/CQDs for reducing Cr(VI) to MIL-53(Fe).

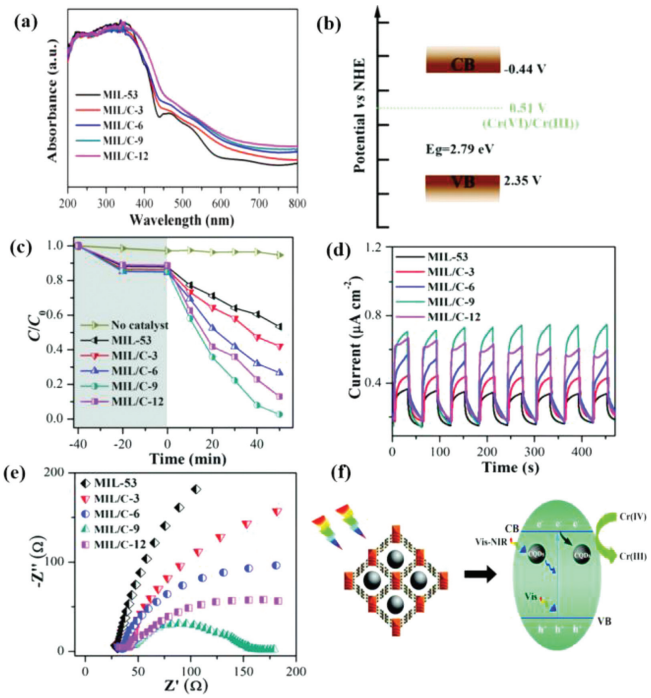

Fig. 4. (a) UV-vis diffuse reflectance spectra (VU-vis DRS) of MIL-53(Fe) and MIL-53/CQDs. (b) Band structure of MIL-53/CQDs. (c) Photocatalytic activities for Cr(VI) reduction of different MIL-53/CQDs composites at pH 4. The photocurrent response (d) and EIS Nyquist plots (e) of MIL-53(Fe) and MIL-53/CQDs. (f) The proposed mechanism of MIL-53(Fe)/CQDs composite for photocatalytic Cr(VI) reduction. Copied with permission [46]. Copyright 2018, the Royal Society of Chemistry.

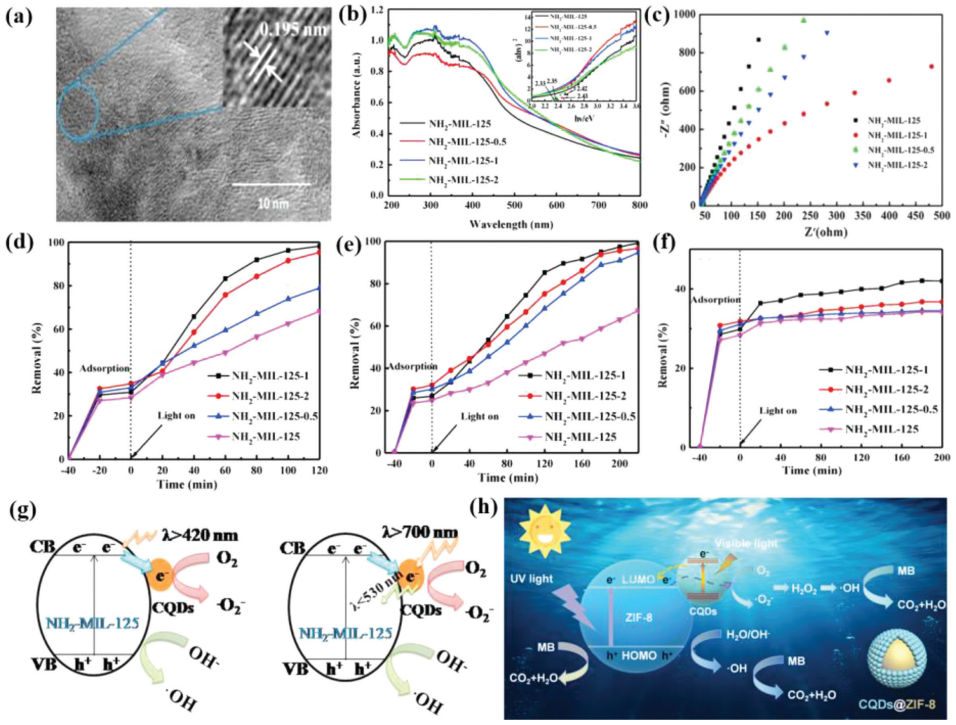

Fig. 5. (a) HRTEM image of CQDs/NH_2-MIL-125. (b) UV-vis DRS and (c) EIS spectra of NH_2-MIL-125 and CQDs/NH_2-MIL-125. Photocatalytic performance of NH_2-MIL-125 and CQDs/NH_2-MIL-125 under (d) the full spectra light, (e) visible light ($\lambda > 420$ nm) and (f) near-infrared light ($\lambda > 700$ nm). The possible photocatalytic degradation process of (g) CQDs/NH_2-MIL-125 toward RhB and (h) CQDs@ZIF-8 toward MB. (a-g) Copied with permission [73]. Copyright 2020, Springer. (h) Copied with permission [57]. Copyright 2019, Elsevier.

The photocatalytic mechanism was illustrated in Fig. 4f. A host of small heterojunction were built with CQDs and metal-oxo clusters in MIL-53(Fe)/CQDs, which can effectively separate the photogenerated electrons and holes originated from MIL-53(Fe) under short-wavelength visible light. Moreover, CQDs as photosensitizers can be sensitized by the visible light to transfer energy toward MIL-53(Fe). In all, the photocatalytic Cr(VI) reduction activity can be efficiently enhanced by the CQDs in MOF pores as both electron acceptors and photosensitizers.

Considering the superior performance toward harvesting and scattering light of N-doped CQDs compared to the pristine CQDs, Qiang *et al.* constructed N-CQD/MOF-5 photocatalyst with "bottle around ship" method for Cr(VI) reduction [72]. N-CQD/MOF-5 has a lower band gap energy (3.41 eV) than that of MOF (3.54 eV), which indicated that the appropriate introduction of N-CQD in MOF-5 can increase the light utilization efficiency by widening the UV light absorption to visible light absorption. Similar with MIL-53(Fe)/CQDs [46], the introduction of N-CQDs can promote the conduction activity of charges by inhibiting the recombination of photogenerated electron-hole pairs. Therefore, the photoreduction efficiency of N-CQD/MOF-5 toward Cr(VI) was 2.5 times higher than that of the pure MOF-5. The photoreduction efficiencies remained stably after the photocatalyst being reused for five cycles.

Besides the Cr(VI) reduction, CD-MOF composites were also used as photocatalysts for organic dyes degradation. Zhang *et al.* introduced CQDs to NH_2-MIL-125 with physical mixing method to construct CQDs/NH_2-MIL-125 photocatalyst [73]. The lattice distance *ca.* 0.195 nm being ascribed to the (002) facet of carbon materials was observed on the surface of CQDs/NH_2-MIL-125 in the HRTEM image (Fig. 5a), confirming the loading of CQDs onto NH_2-MIL-125. Loading of CQDs achieved CQDs/NH_2-MIL-125 a wider visible response range with a lower band gap (2.35 eV) (Fig. 5b) and lower value of R_{ct} (Fig. 5c), which demonstrated boosted photocatalytic RhB degradation activity resulting from the quicker electron-holes separation than that of NH_2-MIL-125. However, overloading of CQDs will block the penetration of light and reduce the photocatalytic efficiency, thus reasonable loading of CQDs content can realize excellent photocatalysis activity of CQDs/NH_2-MIL-125. Above-stated analysis was validated in Figs. 5d and e, in which NH_2-MIL-125 with 1 wt% of CQDs loading (NH_2-MIL-125-1) exhibited the best photocatalytic ability under both full-spectrum and visible light irradiation. In addition, under near-infrared light, CQDs/NH_2-MIL-125 rather than NH_2-MIL-125 could decompose RhB (Fig. 5f), implying that CQDs played a role of spectrum converter in the photocatalysis process to convert the near-infrared photons into visible-light and to enhance the light utilization. The reaction process was described as Eqs. 1-8, and the possible mechanism was proposed in Fig. 5g. Thanks to the enhancement of light energy utilization by CQDs, the electrons on VB of NH_2-MIL-125 could be excited under the full spectra light irradiation and transferred to CB of NH_2-MIL-125, which further were captured by CQDs to react with O_2 molecules for producing $O_2^{\bullet-}$ radicals. Both the produced $O_2^{\bullet-}$ and the holes on NH_2-MIL-125 could react with H_2O to generate $^{\bullet}OH$, which contributed primarily to the degradation of dye molecules.

$$\text{CQDs/NH}_2\text{-MIL-125} + h\nu \rightarrow \text{CQDs/NH}_2\text{-MIL-125} + e^- + h^+ \quad (1)$$

$$e^- + O_2 \rightarrow O_2^{\bullet-} \quad (2)$$

$$O_2^{\bullet-} + H_2O \rightarrow HO_2^{\bullet} + {}^{\bullet}OH \quad (3)$$

$$HO_2^{\bullet} + H_2O \rightarrow H_2O_2 + {}^{\bullet}OH \quad (4)$$

$$H_2O_2 \rightarrow 2{}^{\bullet}OH \quad (5)$$

$$h^+ + OH^- \rightarrow {}^{\bullet}OH \quad (6)$$

$${}^{\bullet}OH + RhB(dye) \rightarrow CO_2 + H_2O \quad (7)$$

$$h^+ + RhB(dye) \rightarrow CO_2 + H_2O \quad (8)$$

CD-MOF composites with core-shell structure were also constructed for the organic dye degradation. Si *et al.* immobilized the prepared CQDs on ZIF-8 surface to fabricate a core-shell structure CQDs@ZIF-8 with ultrasonic hybridization method [57]. The core-shell structure increased the contact area and provided more reaction sites for methylene blue (MB) to accomplish the improved degradation ability. The CQDs@ZIF-8 could remove 91% of MB (initial concentration of 25 mg/L) under 100 min real sunlight irradiation, which is 48% higher than that of the pristine ZIF-8. Moreover, CQDs@ZIF-8 showed a remarkably enhanced removal efficiency of 52% for MB than that of ZIF-8 under visible light. Because the band gap energy of the CQDs@ZIF-8 (4.95 eV) was identical with that of ZIF-8 (4.93 eV), thus the light absorption in visible region was not derived from the electronic transition of the intrinsic band structure of the photocatalyst. It could be contributed to that CQDs, as a photosensitizer, could be excited under visible light to inject electrons into the LUMO of ZIF-8. As illustrated in Fig. 5h, the transferred electrons could react with O_2 molecules to produce $O_2^{\bullet-}$ radicals, which could participate in the reaction to produce ${}^{\bullet}OH$ radicals. Under sunlight irradiation, the electrons from the highest occupied molecular orbital (HOMO) of ZIF-8 could be excited by UV light to the lowest unoccupied molecular orbital (LUMO) of ZIF-8, which might migrate to CQDs to react with O_2 molecules on the surface of CQDs to generate $O_2^{\bullet-}$. Both the produced $O_2^{\bullet-}$ and the h^+ on the HOMO could react with H_2O to generate ${}^{\bullet}OH$ for MB decomposition.

A ternary nanocatalyst, CDs/MIL-88B(Fe)/Bi_2S_3, was constructed by decorating CDs and Bi_2S_3 on a Fe-based MOF (MIL-88B(Fe)) with "ship in a bottle" method for dyes and aromatic compounds degradation [47]. In CDs/MIL-88B(Fe)/Bi_2S_3, the main XRD diffraction peaks of MIL-88B(Fe) remained while the morphology of MIL-88B(Fe) changed from octahedron to spindle-shaped, in which CDs were embedded inside MIL-88B(Fe), and Bi_2S_3 spheres were decorated on CDs/MIL-88B(Fe) surface. The EIS Nyquist plots demonstrated that CDs/MIL-88B(Fe)/Bi_2S_3 possessed a higher charge ternary separation efficiency than those of MIL-88B(Fe) and Bi_2S_3. The nanocatalyst with high durability and stability can degrade both cationic MB and anionic acid blue 92 (AB92) dyes under visible light by enhancing the separation of electron-hole pairs, which demonstrated higher degradation efficiencies than Bi_2S_3, CDs/MIL-88B(Fe), and MIL-88B(Fe). The mechanism can be illustrated as Eqs. 9-16, indicating that $O_2^{\bullet-}$ and ${}^{\bullet}OH$ were the important factors for the degradation of dyes. Besides, CDs/MIL-88B(Fe)/Bi_2S_3 could also perform as a catalyst for reducing 4-nitrophenol (4-Nip) to 4-aminophenol (4-Amp) due to the synergic effect between CDs and Bi_2S_3.

$$CDs/MIL\text{-}88B(Fe)/Bi_2S_3 + h\nu \rightarrow CDs/MIL\text{-}88B(Fe)/Bi_2S_3(e_{CB}^- + h_{VB}^+) \quad (9)$$

$$e_{CB}^- + O_2^{\bullet-} + 2H^+ \rightarrow H_2O_2 \quad (10)$$

$$H_2O_2 + O_2^{\bullet-} \rightarrow {}^{\bullet}OH_{ads} + O_2 + OH^- \quad (11)$$

$$h_{VB}^+ + OH_{ads}^- \rightarrow {}^{\bullet}OH_{ads} \quad (12)$$

$$h_{VB}^+ + H_2O \rightarrow {}^{\bullet}OH_{free} + H^+ \quad (13)$$

$$H_2O_2 + e_{CB}^- \rightarrow {}^{\bullet}OH_{ads} \quad (14)$$

$$OH^- + h_{VB}^+ \rightarrow {}^{\bullet}OH_{ads} \quad (15)$$

$${}^{\bullet}OH_{ads} + O_2^{\bullet-} + dye \rightarrow \text{degradation products} \quad (16)$$

CD-MOF composites in film form have been fabricated and used for catalytic degradation of pollutants [74,75]. Safa *et al.* assembled the UiO-66-NH_2 and graphene quantum dot (GQDs) on a non-woven polypropylene substrate (NM-PP) to fabricate GQDs/UiO-66-NH_2/NW-PP by binding GQDs with UiO-66-NH_2 through hydrogen bonding interactions [74]. GQDs/UiO-66-NH_2/NW-PP could promote the photocatalytic MB degradation by reducing the recombination of photo yield electron/hole pairs. In their another work, UiO-66-NH_2 and GQDs were assembled on a AISI 304 stainless steel mesh plate precoated with ZnO thin film [75]. For the photosensitivity promotion by GQD and the inhibition for the photoexcited charge pairs recombination, the obtained AISI steel/ZnO/UiO-66-NH_2/GQDs could degrade long chain oleic acid to small molecules under UV light.

3.2. Energy production

Splitting water (H_2 evolution) and reducing CO_2 (CO and CH_4 evolution) by photocatalysis are considered as two of the most efficient and sustainable way for green energy production [76,77]. Recently, CD-MOF composites have been aroused researchers' attentions in photocatalytic splitting water and reducing CO_2. Recent examples in energy production with CD-MOF composites as photocatalysts are discussed below and summarized in Table 2.

Zhang *et al.* co-introduced CDs and CdS quantum dots into MIL-101 to fabricate a ternary CD/CdS@MIL-101 photocatalyst for H_2 evolution without noble metal participation [48]. The preparation process and morphology were depicted in Ship in a bottle section. The photocatalytic H_2 evolution performance in aqueous solution of lactic acid was studied. Under visible light, the light-harvester CdS absorbed light and generated electrons, and the generated electrons in the conduction band (CB) were transferred to the CB of MIL-101. With the existence of CDs, the photoinduced electrons can be more effectively collected and transported from the CB of MIL-101 to H^+. The H^+ could be effectively reduced to H_2, and the leaving holes in VB can be captured by lactic acid. Being confirmed by the Nyquist curves and photocurrent measurements, the photogenerated charges separation efficiency was effectively improved. Thus, the maximum H_2 production rate of CD/CdS@MIL-101 can reach 14.66 μmol/h, which is *ca.* 8.5 and 18.6 times higher than thoseof CdS@MIL-101 and CdS, respectively.

Zheng *et al.* introduced carbon nitride quantum dots (g-CNQDs) to a two-dimensional (2D) ultrathin porphyrin MOF (PMOF) to fabricate a hybrid catalyst (g-CNQDs/PMOF) for facilitating the activity of photocatalytic CO_2 reduction to CH_4 and CO [78]. The nitrogen atoms in 0D g-CNQDs can directly coordinated with the unsaturated Co sites in 2D PMOF, which shortened the migration pathways of both photo-generated charge carries and gaseous substrates from g-CNQDs to cobalt active centers. The strong fluorescence emission of g-CNQDs was quenched with the presence of PMOF, and the energy transfer process (τ_3) related to the electron transferred from g-CNQDs to PMOF occupied the highest percentage (feeding ration of g-CNQDs:PMOF = 1:6), indicating that both the effective electron transfer from g-CNQDs to PMOF along with the effective separation performance of photogenerated

Table 2
CD-MOF composites for energy production.

Photocatalyst	Synthesis method	Applications	Light source	Evolution rate	Cycles	Role of CDs	Ref.
CD/CdS@MIL-101	Ship in a bottle	H_2 evolution	Visible light	14.66 μmol/h	4	Charge collector	[48]
g-CNQDs/PMOF	Physical mixing	CO and CH_4 evolution	Visible light	16.1 μmol g^{-1} h^{-1} (CO); 6.86 μmol g^{-1} h^{-1} (CH_4)	-	Donator of lone electron paris to coordinate with PMOF and capture CO_2	[78]
CD@NH_2-UiO-66	Bottle around ship	CO evolution	Visible light	16.6 μmol g^{-1} h^{-1}	10	Electron receptors, photosensitizers	[43]
Zn-Bim-His-1@GQDs	Physical mixing	CO and CH_4 evolution	Visible light	3.7 μmol g^{-1} h^{-1} (CO); 20.9 μmol g^{-1} h^{-1} (CH_4)	4	Photon harvesting unit	[79]

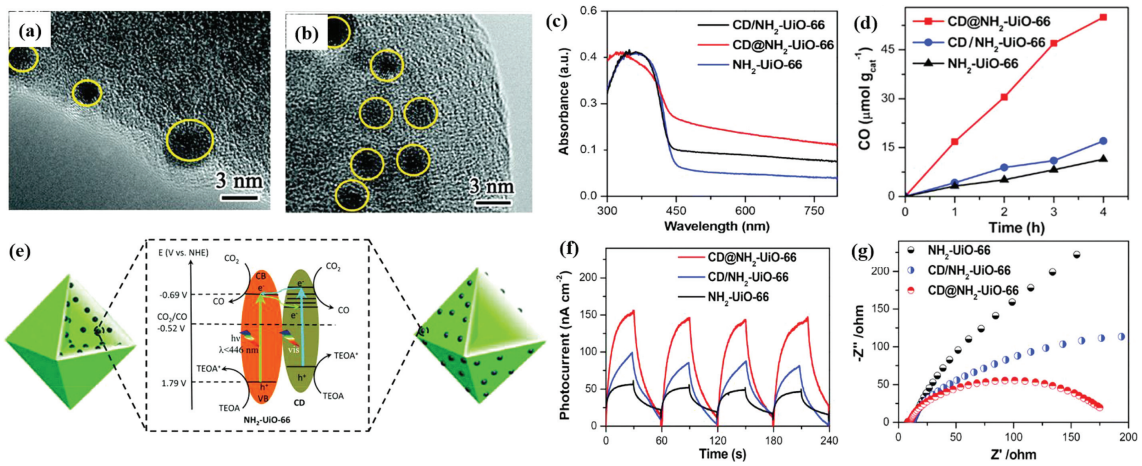

Fig. 6. TEM images of CD/NH_2-UiO-66 (a) and CD@NH_2-UiO-66 (b). (c) UV-vis DRS. (d) production rate of CO. (e) Scheme of the photocatalytic mechanism. (f) Photocurrent and (g) EIS Nyquist plots of pristine NH_2-UiO-66, CD/NH_2-UiO-66 and CD@NH_2-UiO-66. Copied with permission [43]. Copyright 2020, the Royal Society of Chemistry.

electron-hole pairs led to a better photocatalytic performance of g-CNQDs/PMOF than that of g-CNQDs and PMOF. Under visible light irradiation, the Co(II) captured the electrons form Co(I), and the holes were consumed by the sacrificial reagent triethanolamine (TEOA). The active Co(I) center reduced CO_2 to CO, and then be oxidized to Co(II). CO can be further reduced to the eight-electron production CH_4 with the concerted proton coupled electron transfers (PCETs). The evolution efficiency of CO and CH_4 were 16.1 and 6.86 μmol g^{-1} h^{-1}, which were 2.34 and 6.02 times higher than that of bare PMOF, respectively.

Li *et al.* explored the effect of the CDs position on the photocatalytic property of CD-MOF composites [43]. They decorated CDs on NH_2-UiO-66(Zr) surface to obtain CD-decorated (CD/NH_2-UiO-66) (Fig. 6a) and encapsulated CDs into NH_2-UiO-66(Zr) to fabricate the CD embedded NH_2-UiO-66 particles (CD@NH_2-UiO-66) (Fig. 6b), which can be clearly verified by high-resolution TEM images. The UV-vis DRS (Fig. 6c) indicated that both CD/NH_2-UiO-66 and CD@NH_2-UiO-66 exhibited obvious light response under the visible light, in which the light response of CD@NH_2-UiO-66 was stronger. It can be contributed to that the internal CDs in CD@NH_2-UiO-66 can absorb a large amount of incident light scattered inside MOF pores. The photocatalysis investigation showed that CD@NH_2-UiO-66 (16.6 μmol g^{-1} h^{-1}) exhibited a better CO_2 reduction capacity than that of CD/NH_2-UiO-66(4.0 μmol g^{-1} h^{-1}) (Fig. 6d). The corresponding photocatalysis mechanism was proposed in Fig. 6e. Under the light $\lambda < 440$ nm, NH_2-UiO-66 could be excited by the light to generate electron-hole pairs. The CDs acted as electron receptors to improve the production rate of CO, which were proved by the photocurrents (Fig. 6f) and EIS data (Fig. 6g). Moreover, the CDs encapsulated inside NH_2-UiO-66 can directly contact with the internal Zr-O clusters and form many heterojunctions, which further enhanced the charge separation. As well, under the irradiation of long-wavelength light, CDs can harvest the light and act as photosensitizers to generate more electron-hole pairs.

Considering the influence of the CDs position on the photocatalytic performance of CD-MOF composites, Wei *et al.* mounted GQDs into the holes of a Zn based MOF (Zn-Bim-His-1) with lots defective hole structures on the surface to construct Zn-Bim-His-1@GQD heterostructures for efficient photocatalytic CO_2 reduction [79]. Under visible light, Zn-Bim-His-1@GQDs showed the higher CH_4 production rate than those of the pristine Zn-Bim-His-1 and GQDs. In addition, water is essential for protons providing in the conversion reaction of CO_2 to CH_4, in which the appropriate pH value is beneficial to the photocatalytic process. By analyzing the photocurrent response, electrochemical impedance spectroscopy (EIS) results and the photocatalytic performances, it was found that the rich interfaces between GQDs and Zn-Bim-His-1 with the formed heterojunctions can effectively improve both the separation and mobility of the charge carriers to promote the CO_2 reduction.

4. Application in sensing

Although MOFs with intrinsic luminescence have been widely studied in fluorescent sensing, their applications are still restricted by low quantum yields and limited charge transfer between metal ions/clusters and ligands [80]. Therefore, efforts have been made to construct fluorescent sensors by introducing fluorescence guests in MOFs. For instance, our research group has fabricated MOFs-based composites like RhB@ZIF-8 (RhB: rhodamine B) and FSS@ZIF-8 (FSS: fluorescein disodium salt) [20], Eu@BUC-14 (BUC: abbreviation of Beijing University of Civil Engineering and Architecture)

Table 3
Synthesis method and application of CD-MOF composites based luminescent sensors.

Sensor	Synthesis method	Method	Analytes	LOD	Real samples	Ref.
C-dots@UMCM-1a	Physical mixing	Fluorescence quenching	NB, TNP		-	[94]
amine-CQDs@UiO-66	Physical mixing	Fluorescence quenching	4-NP	3.5 nmol/L	-	[54]
BPEI-CQDs/ZIF-8	Bottle around ship	Fluorescence quenching	Cu^{2+}	80 pmol/L	River water	[44]
CDs@Eu-DPA MOFs	Bottle around ship	Ratiometric fluorescent sensing	Cu^{2+}	26.3 nmol/L	River water	[86]
Eu^{3+}/CDs@MOF-253	Bottle around ship	Ratiometric fluorescent sensing	Hg^{2+}	13 ppb	River water; fountain water	[87]
CDs@Eu-MOF	Bottle around ship	Ratiometric fluorescent sensing	Cr(VI)	0.21 μmol/L	Tap water; river water; stream	[90]
CDs@MOF(Eu)	Bottle around ship	Fluorescence quenching	Doxycycline	0.36 μmol/L	Simulated biological system	[52]
		Ratiometric fluorescent sensing	MnO_4^-	0.36 μmol/L	Tap water	
CDs@UiO-66-$(OH)_2$	*In situ* encapsulated	Fluorescence quenching	Fe^{3+}	0.76 μmol/L	-	[58]
			Temperature	-		
			pH	-		
CDs@ZIF-90	Bottle around ship	Ratiometric fluorescent sensing	PO_4^{3-}	0.23 μmol/L	Tap water, lake water	[89]
CDs@ZIF-8	Bottle around ship	Fluorescence quenching	QCT	3.5 nmol/L	Real wine sample	[49]
CDs@ZIF-8@MIP	Physical mixing	Fluorescence quenching	QCT	2.9 nmol/L	Ginkgo biloba extract capsules	[55]
EuMOFs/CD@CMC	Physical mixing	Ratiometric fluorescent sensing	OP	89 nmol/L	The skin surface of different fruits and vegetables	[56]
Eu-MOF/N, S-CD	Bottle around ship	Ratiometric fluorescent sensing	Water	0.03%	-	[53]
Tb^{3+}@p-CDs/MOF	Bottle around ship and physical mixing	Ratiometric fluorescent sensing	Water/relative humidity	0.28% in ethanol; 0.33% in DMF; 0.25% in cyclopropane	-	[98]
CNDs@ZIF-8-3	Calcine ZIF-8 for 3 h	Fluorescence quenching	Temperature	-	-	[59]
C-QDs@UiO-66-$(COOH)_2$ film	Physical mixing and electrophoretic deposition	Fluorescence quenching	Temperature	-	-	[99]
Eu^{3+}/C-dots@MIL-53	Bottle around ship and physical mixing	Ratiometric fluorescent sensing	TDA	6.8 μg/mL	-	[96]
BYCDs@ZIF-8	Bottle around ship	Ratiometric fluorescent sensing	GSH	0.9 nmol/L	Grape, cucumber	[97]

[19], SQDs@UiO-66-NH_2 (SQD: sulfur quantum dots) [21] for water pollutant sensing. Recently, CDs with unique optical properties have become one of the most popular guests for constructing MOF-based composites sensors [42]. On the basis of signal transduction, CD-MOF composites-based sensors have been reported and they include two main types: optical and electrochemical. Taking the advantage of both high quantum yield of the CD and MOF's luminescent emission and the high selective adsorption and efficient accumulation towards target analytes of the host MOF with ultrahigh porosities and surface areas, it was expected that CDs-MOF composites displayed outstanding photoluminescence activities. The interesting part is that the assembly of CD with MOF can enhance the electrochemical sensing performance.

4.1. Luminescence sensors

Besides the potential of using CD-MOF composites in photocatalysis, numerous researchers have devoted to construct CD-MOF composites for fluorescent sensing applications (Table 3). It is worth mentioning that the ratiometric fluorescent sensor based CD-MOF with dual emission or multiple emission centers can be constructed *via* screening CD and MOF materials, whose detection accuracy can be improved by reducing the interference of excitation source fluctuation, background absorption, and probe concentration.

4.1.1. Gas sensing

With properties including high specific surface area, large porosity, and optical property, MOFs have become a promising candidate for sensing gas molecules [81–85]. Recently, sensing gas molecules with a sensor based on CD-MOF composites has captured the attention of researchers. Considering the ratiometric sensors are more accurate and more helpful in eliminating interferences such as background fluorescence and probe concentration, Gao *et al.* fabricated a ratiometric sensor for sensing H_2S in the aqueous phase (CDs@ZIF-8@GMP/Tb), in which the fluorescence of CDs and Tb respectively acted as the reference signal and the response signal [50]. CDs@ZIF-8@GMP/Tb was prepared by imbedding CDs in ZIF-8 with "bottle around ship" strategy firstly and then coated with the guanosine monophosphate (GMP) modified terbium ions (Tb^{3+}), which exhibited the distinct fluorescence emission of CDs (450 nm) and Tb^{3+} (485, 545, 584, 623 nm) under the excitation with 300 nm UV light, respectively. With the addition of Cu^{2+} in aqueous solution of CDs@ZIF-8@GMP/Tb, Cu^{2+} coordinated with GMP and replaced Tb^{3+}, thus quenching the fluorescence of Tb^{3+} but not affecting the fluorescence of CDs. On this basis, CDs@ZIF-8@GMP/Tb with Cu^{2+}-mediated fluorescence was employed as a H_2S sensor in *N*-2-hydroxyethylpiperazine-*N*′-2-ethanesulfonic acid (HEPES) buffer with pH 7.4. As a result, fluorescence of Tb^{3+} was enhanced with the presence of H_2S because of the interaction between Cu^{2+} and H_2S, while no obvious change was observed with the fluorescence of CDs. With the increase of

H_2S concentration, the ratio of emission intensity at 545 and 450 nm (F_{545}/F_{450}) increased, and demonstrated a good linear relationship in the range from 0.5 μmol/L to 100 μmol/L with a LOD of 150 nmol/L. It is worth noting that the sensing property of CDs@ZIF-8@GMP/Tb can be reversed with alternate addition of Cu^{2+} ions and H_2S after three cycles and cannot be interfered by some coexisting anions, thiols and biological species.

4.1.2. Ions sensing

Various pollutants exist in ionic form in polluted water, so the detection of anions and cations is significant for protecting water. At present, researches on sensing ions in water with CD-MOF composites-based sensors mainly focus on metal cations, nutrient ions and toxic anions containing metal elements. In this section, representative studies are reviewed and discussed, which can provide effective guidance for the design and application of CD-MOF based sensors in ions sensing.

Heavy metal cations: Generally, the heavy metal ions were difficult to be biodegraded but easy to be accumulated in organisms through food chain, which might exert severe threat to the ecosystem and human health. Iron ion is an essential trace element for human and animals, but excessive intake can cause chronic poisoning. Water body will become turbid with the concentration of iron ion exceeding 0.3 mg/L and will emit a foul odor with the concentration exceeding 1.0 mg/L. By encapsulating CDs in UiO-66-$(OH)_2$, Yao *et al.* fabricated CDs@UiO-66-$(OH)_2$ composites with strong fluorescence at 464 nm ascribing from CDs for Fe^{3+} sensing in aqueous solution [58]. With the increase of Fe^{3+} concentrations, the fluorescence intensities of CDs@UiO-66-$(OH)_2$ decreased due to the collisional quenching mechanism. In the range of 100-800 μmol/L, the quenching effect was linear with the concentration. LOD of Fe^{3+} with this sensor was calculated as 0.76 μmol/L, indicating the feasibility of Fe^{3+} sensing with CDs@UiO-66-$(OH)_2$. In addition, the sensor can be used in temperature and pH measurement.

Copper ions (Cu^{2+}) are essential to animals and human beings, but excessive Cu^{2+} ions are toxic. Lin *et al.* constructed BPEI-CQDs/ZIF-8 composites with bright blue emission (440 nm) under 365 nm UV-light [44]. By adding Cu^{2+} in BPEI-CQDs/ZIF-8 suspension, the strong blue emission of BPEI-CQDs/ZIF-8 was quenched because of the fluorescence inactive complex formed by the Cu^{2+} and BPEI-CQDs. In addition, BPEI-CQDs/ZIF-8 exhibited excellent adsorption ability towards Cu^{2+} due to the cation-adsorption properties of ZIF-8 and the complexation of Cu^{2+} and imidazole, thus exhibiting a higher quenching efficiency than that of BPEI-CQDs. Different from the above work, Hao *et al.* fabricated CDs@Eu-DPA MOFs (DPA = 2,6-pyridinedicarboxylic acid) for Cu^{2+} ratiometric detection with the fluorescence signal of CDs as reference [86]. Due to a stronger coordination ability towards DPA than Eu^{3+}, Cu^{2+} can replace Eu^{3+} to coordinate with DPA, thus breaking the energy transfer from DPA to Eu^{3+} and quenching the fluorescence of Eu^{3+} (F_{615}). However, the fluorescence of CDs (F_{425}) was not affected by the presence of Cu^{2+}. Thus, F_{425}/F_{615} was used as the signal in Cu^{2+} detection in this work and 26.3 nmol/L LOD was obtained in the concentration range of 50 nmol/L $\sim$ 10 μmol/L.

Hg(II) ion also exerted serious threat to human health and environment. Xu *et al.* fabricated a hybrid (Eu^{3+}/CDs@MOF-253) with a faint blue light and used it as a ratiometric sensor for Hg^{2+} sensing in water [87]. With the co-existence of Hg^{2+}, the fluorescence signal of Eu^{3+}/CDs@MOF-253 in water altered from blue to red under UV light because Hg^{2+} could coordinate with the functional groups in CDs and quench its fluorescence, while the fluorescence of Eu^{3+} was not affected. The relative fluorescence intensities (I_{Eu}/I_{CD}) were linearly correlated with the Hg^{2+}concentration in the range of 0-150 μmol/L, in which the LOD was 13 nmol/L. Moreover, the sensing performance of Eu^{3+}/CDs@MOF-253 towards Hg^{2+} was not interfered by other common ions such as Zn^{2+}, Ni^{2+}, Na^{+} in water environment, implying potential application in real water environment.

Anions: Phosphate, as an inorganic anion, can cause severe water pollution when its concentration exceeds a certain limit [88]. The detection of phosphate is significant for avoiding water pollution. With the combination of the blue fluorescence signal of CDs and the scattering signal of ZIF-90, a ratiometric sensor for phosphate detection was recently reported [89]. CDs@ZIF-90 was fabricated with "bottle around ship" method, in which Zn^{2+} was firstly adsorbed on the CDs with negative charge and then coordinated with imidazole-2-carboxaldehyde (2-ICA) to form ZIF-90. Under UV light of 365 nm, the fluorescence intensity at 440 nm (F_{440}) of CDs@ZIF-90 was suppressed compared with CDs alone, while the scattering intensity (S_{732}) was improved because of the increase of the CDs@ZIF-90 size. As depicted in Fig. 7a, the PO_4^{3-} could replace 2-ICA to coordinate with Zn^{2+}, destroying the framework of ZIF-90 and releasing CDs, which led to the increase of F_{440} and the decrease of S_{732} (Fig. 7b). The framework destruction of ZIF-90 with the presence of PO_4^{3-} could be proved by the SEM (Figs. 7c and d) and XRD patterns (Fig. 7e) of CDs@ZIF-90 and CDs@ZIF-90 after contact with PO_4^{3-}. Thus, CDs@ZIF-90 could be used as a ratiometric sensor for PO_4^{3-} sensing, in which the F_{440}/S_{732} showed a linear relation with PO_4^{3-} changing in the concentration range of 1.0-50.0 μmol/L with a LOD of 0.23 μmol/L. Fluorescence and scattering signal change with the addition of PO^{3-} under 365 nm UV light can be observed with naked eyes (Fig. 7f). Further studies found that F_{440}/S_{732} signal change could be limited in acidic and high alkalinity condition, which were respectively attributed to the protonation of PO_4^{3-} and the competition between PO_4^{3-} and OH^- to react with Zn^{2+}. It was confirmed that CDs@ZIF-90 could effectively detect PO_4^{3-} in aqueous solution in the pH range of 6.0-9.0. In addition, CDs@ZIF-90 could selectively detect PO_4^{3-} among 14 other metal ions (Mg^{2+}, Hg^{2+}, Fe^{3+}, Cu^{2+}, Cd^{2+}, Ca^{2+}, Mn^{2+}, Co^{2+}, Ni^{2+}, Cr^{3+}, Ba^{2+}, Pb^{2+}, Na^{+}, and K^{+}) and three other anions (CO_3^{2-}, ClO^-, and $S_2O_3^{2-}$), indicating that this CDs@ZIF-90 sensor can be used to detect PO_4^{3-} concentration in the real water samples.

CD-MOF composites were also fabricated to sense other anions such as MnO_4^- and $Cr_2O_7^{2-}$ in water environment. For example, Fu *et al.* employed CDs@MOF(Eu) composites to detect MnO_4^- in aqueous solutions with fluorescence quenching, which can be explained by the energy transfer between MOF(Eu) and MnO_4^- and the interaction of MnO_4^- with CDs and MOF(Eu) [52]. LOD was calculated as 0.68 μmol/L, which was lower than that of MOF(Eu) alone in the detection process. Tap water was used to study the detection of MnO_4^- in real environmental samples, in which the satisfactory recoveries and relative standard deviation (RSD) were obtained, indicating the reliability of CDs@MOF(Eu) in MnO_4^- detection in real samples.

Wang *et al.* designed a fluorescent ratiometric sensor (CDs@Eu-MOFs) for $Cr_2O_7^{2-}$ sensing in aqueous solution [90] by a different mechanism with Fu's work mentioned above [52]. Under the irradiation with 390 nm UV light, CDs@Eu-MOFs exhibited a noticeable emission peak at 467 nm originating from CDs and two weak emission peaks at 590 and 616 nm originating from the Eu^{3+} in Eu-MOFs. With the presence of $Cr_2O_7^{2-}$, fluorescence emission of CDs@Eu-MOFs at 467 nm was quenched by Cr(VI), while the emission intensity at 616 nm was almost unchanged. The fluorescence ratio (F_{467}/F_{616}) of CDs@Eu-MOFs showed a linear relationship with $Cr_2O_7^{2-}$ concentration in the range from 2 μmol/L to 100 μmol/L, and LOD was calculated as 0.21 μmol/L. No interference for F_{467}/F_{616} was found with other 15 common metal ions being added in the aqueous solution of CDs@Eu-MOFs, indicating excellent selectivity in Cr(VI) sensing. The lifetime of CDs combined with $Cr_2O_7^{2-}$ was consistent with that of CDs, indicating the

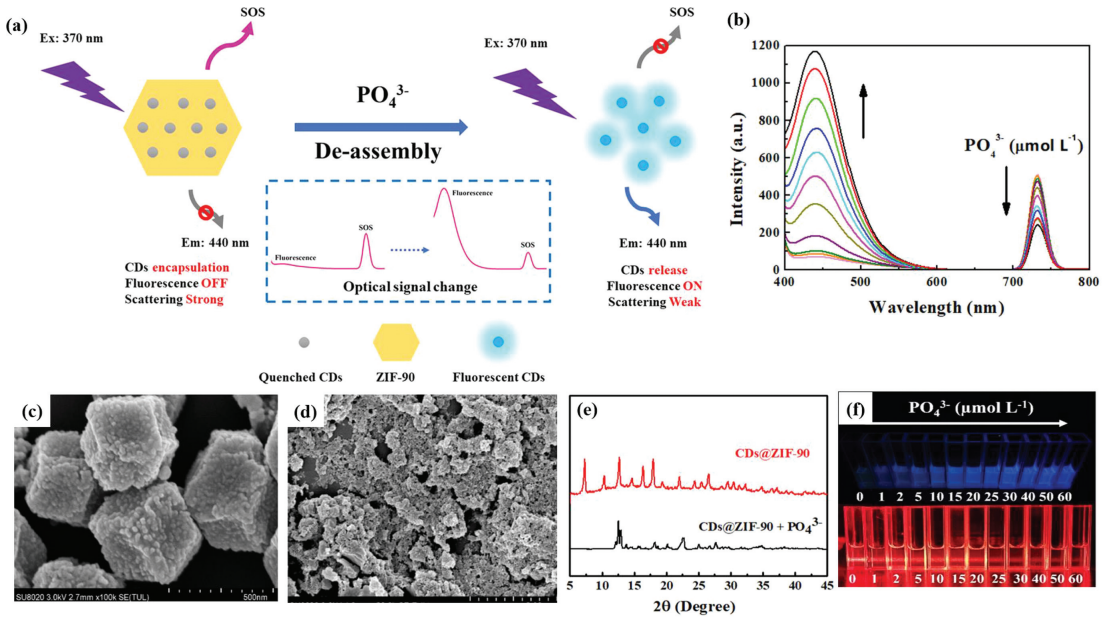

Fig. 7. (a) Mechanism of the PO_4^{3-} sensing with CDs@ZIF-90. (b) Fluorescence and scattering signal change with different PO_4^{3-} concentrations. SEM images of (c) CDs@ZIF-90 and (d) CDs@ZIF-90 + PO_4^{3-}. (e) XRD patterns of CDs@ZIF-90 and CDs@ZIF-90 + PO_4^{3-}. (f) Photographs of the mixture solution of CDs@ZIF-90 and PO_4^{3-} under 365 nm UV light and laser. Copied with permission [89]. Copyright 2020, American Chemical Society.

quenching process was a static without any energy transfer. Further analysis revealed that the high sensitivity for $Cr_2O_7^{2-}$ sensing was due to the inner filter effect of Cr(VI) and the strong adsorption capacity of $Cr_2O_7^{2-}$ with Eu-MOFs. In addition, CDs@Eu-MOFs were expected to function even in real water samples such as tap water, river water and stream with satisfactory recoveries in the range of 91.9%-110.62% and RSD in the range of 0.69%-1.57%.

4.1.3. Organic contaminants

A large number of organic chemicals have been found to pollute the environment through industrial processes such as textile, printing, steel, petroleum, pesticide, paint, and medicine. Although the chemical composition of these chemicals varies greatly in molecular weight and toxicity, most of them are highly toxic, highly cumulative and difficult to degrade, which will damage the ecosystem and human health. Common organic pollutants include phenols, aniline, nitrobenzene, organophosphorus pesticides and so on. As these pollutants are harmful to organisms even at low concentrations, their timely and effective detection is particularly important. Currently, CD-MOF composites-based sensors have been affirmed to be a promising option for organic pollutants detection.

Volatile organic compounds (VOC) (hydrocarbons, benzene and derivatives, *etc.*), which are usually toxic and carcinogenic to human beings and animals, are common contaminants in water and air environment [91–93]. Weng *et al.* constructed a dual-emission N-GQDs/Eu^{3+}@Mg-MOF hybrid as platform to detect a series of atmospheric benzene homologues (BTEX) [51]. When being excited at 349 nm, N-GQDs/Eu^{3+}@Mg-MOF showed two emission signals respectively from the linker 1,4-naphthalenedicarboxylate (1,4-ndc) and Eu^{3+}. Fluorescence life time of N-GQDs/Eu^{3+}@Mg-MOF decreased with the exposure of a series of BTEX, indicating the energy transfer process between the 1,4-ndc and Eu^{3+} can be disturbed by the guest molecules. The ratio of the above two emission intensity (I_L/I_{Eu}) could be used to distinguish toluene and phenylethane vapors, but could not be used distinguish benzene and m-xylene because of their similar structures. When being excited at 394 nm, N-GQDs/Eu^{3+}@Mg-MOF showed a dual-emission originating from N-GQDs and Eu^{3+} respectively, and the ratio of the two emissions intensities ($I_{Eu}/I_{N\text{-}GQDs}$) changed with the exposure to different BTEX. However, the ratio failed to be used to distinguish benzene and toluene. Therefore, the author established a dual-readout orthogonal identification scheme with the value I_L/I_{Eu} as abscissa and $I_{Eu}/I_{N\text{-}GQDs}$ as ordinate, which could be used to separate those readouts and well distinguish those BTEX with the 2D readouts (I_L/I_{Eu}, $I_{Eu}/I_{N\text{-}GQDs}$). In other words, a database could be established with enough targeted compounds based on this work.

Explosive and explosive-like substances with high toxicity and refractory have become contaminants in aquatic systems. Li *et al.* prepared carbon nanodots (Cdots) functional UMCM-1 composites (Cdots@UMCM-1a) with high fluorescence for nitrobenzene (NB) and 2,4,6-trinitrophenol (TNP) detection [94]. Characterization of Cdots@UMCM-1a proved that Cdots was well-dispersed in UMCM-1a with the integrity of the crystal structure of UMCM-1a remained. Green luminescence of Cdots@UMCM-1a originates from Cdots and can be stable at laboratory conditions for more than 30 d. With NB and TNP being added, electron on the amino groups of Cdots transferred to NB or TNP molecules, causing the fluorescence of Cdots@UMCM-1a to be quenched quickly. Moreover, due to the synergistic effect of UMCM-1 and Cdots, Cdots@UMCM-1a is more sensitive in sensing NB and TNP than that of Cdots alone.

Similarly, Yang *et al.* fabricated an amine-CQDs@UiO-66 composite by post modification method to sense 4-nitrophenol (4-NP) in water [54]. Amine-CQDs@UiO-66 composites remained the morphology and crystal structure of UiO-66, and showed a strong blue FL emission (λ_{em} = 440 nm) ascribing to amine-CQDs (λ_{em} = 444.5 nm) excited at 365 nm. UiO-66 and amine-CQDs can selectively adsorb phenol compounds and selectively sense 4-NP, respectively. It was expected that the amine-CQDs@UiO-66 might selectively sense 4-NP among other nitrophenol analogs (2,4-dinitrophenol (DNP), trinitrophenol (TNP), and phenol (PHE)) and metal ions with florescence quenching. Quantitative detection experiments indicated that the fluorescence quenching was in a linear relationship with the concentration of 4-NP in 0.01-20 μmol/L, in which the LOD was calculated as 3.5 nmol/L.

Antibiotics are also common pollutants in water environment because they are extensively used and can hardly be degraded.

The above-mentioned MnO_4^- sensor material in Anions section, CDs@MOF(Eu) composite, can also be employed as a fluorescent sensor for doxycycline sensing [52]. Because the adsorption peak of doxycycline can overlap the emission peak of CDs at 436 nm, and doxycycline can combine with Eu^{3+}, fluorescence of CDs was quenched while fluorescence of MOF(Eu) at 616 nm was enhanced with the presence of doxycycline. With the increasing doxycycline concentration, the values of $\ln(F_{616nm}/F_{436nm})$ grew and showed a linear relationship with the LOD of 0.36 μmol/L. Further studies showed that the detection of doxycycline with CDs@MOF(Eu) was not interfered by other antibiotics. Moreover, a test paper fabricated from the CDs@MOF(Eu) was prepared and showed the color change from blue-purple to pink-red under an addition of 365 nm UV light with doxycycline.

Quercetin (QCT) is a widely used drug for antioxidant, anti-inflammatory, antiviral, anti-arrhythmia, anti-blood platelet [95]. By embedding carbon dots in ZIF-8, a highly luminescent composites (CDs@ZIF-8) were constructed for QCT detection [49]. After adding CDs@ZIF-8 into QCT solution, the 3-hydroxyl group on QCT interacted with the basic groups at the surface of CDs in ZIF-8 by electrostatic interaction to form a new complex, which could be proved by the appearance of the new peak in UV absorption band. The new peak located in the fluorescence emission interval of the CDs, increasing the energy transfer from CDs@ZIF-8 to QCT, which was highly sensitive and selectively sensing toward QCT *via* the fluorescence quenching. Based on the Stern-Volmer equation and three parallel fluorescence determination of blank solutions, the theoretical LOD of QCT could reach 3.5 nmol/L. The combination of CDs and ZIF-8 improved the sensitivity and selectivity significantly, which reduced the potential interferences including other analogues of QCT and some common metal ions. In addition, the authors verified the reliability of CDs@ZIF-8 in detecting QCT in real wine sample, and obtained well consistent results with the comparation of HPLC-UV. To further improve the selectivity towards QCT, they embedded CDs in ZIF-8 and combined molecular imprinting method to construct sensor (CDs@ZIF-8@MIP) in another work [55]. No obvious difference was found between the absorption spectrum of CDs@ZIF-8@MIP with the addition of QCT and the stacked spectrum of CDs@ZIF-8@MIP and QCT, indicating no energy transfer. Further analysis indicated the dynamic process of inner filter effect generated between CDs@ZIF-8@MIP and QCT, which resulted into the fluorescence intensity to decrease dramatically. Moreover, ZIF-8 is an ideal platform for MIP membrane forming and allows the release of more imprinted sites from the deep buried polymer networks than the CDs@MIP, thus improving the binding ability and mass transfer rate. Results showed that the detection process followed a linear relationship in the range of 0-50 μmol/L with an LOD of 2.9 nmol/L. The CDs@ZIF-8@MIP exhibited higher selectivity towards QCT than other analogs due to the synergistic effect of CDs and the specific binding sites provided by MIP. Further study showed that this sensor can be applied in sensing QCT in real samples of Ginkgo biloba extract capsules from different manufacturers with good accuracy.

Chlorpyrifos (CP) as a typical phosphorus pesticide (OP), poses significant risk to human beings and animals. It was essential to conduct the detection of residual CP is very important. For real-time and more accurate detection of CP, Xu *et al.* fabricated a ratiometric fluorescent glove sensor (EuMOFs/CDs@CMC) by integrating a flexible host material (CMC aerogel) with two fluorescent centers of EuMOFs and CDs [56]. The ratiometric fluorescent sensor displayed two fluorescence emission bands from Eu^{3+} and CDs, in which EuMOF was used as the CP sensing receptor and CDs as a reference fluorescence center. Under 365 nm UV irradiation, the glove emitted red color from Eu^{3+}, while after swiping the surface of apple with CP, a blue color appeared. With the presence of CP, both of the crystalline structure and the emission lifetime monitored at 313 nm of EuMOF were remained, indicating no interaction between CP and Eu^{3+}. The UV-vis spectra of the ligand BTB (1,3,5-benzenetribenzoic acid) was mostly covered by that of CP, indicating that the CP could filter the light adsorbed by MOF ligand, and disturb the energy transfer from the ligand to Eu^{3+}, thus resulting to the fluorescence of Eu^{3+} quenching. A linear relationship of the relative fluorescence intensities (F_{CDs}/F_{Eu}) was found towards the CP detection in the range of 5-40 μmol/L with the LOD of 89 nmol/L.

4.1.4. Biomakers

CD-MOF composites as fluorescent sensors also presented promising application in sensing biomarkers including diaminotoluene (TDA) and glutathione (GSH) [96,97]. Toluene diisocyanate (TDI) is considered as one of the most common causes of occupational asthma. The concentration of TDA (a detectable metabolite of TDI in urine), is closely linked to TDI, was chosen as a biomarker to evaluate the sources of TDI. Recently, a CD-MOF based ratiometric sensor, Eu^{3+}/C-dots@MIL-53, was developed by Qin and Yan for TDA sensing [96]. C-dots were encapsulated in MIL-53-COOH with "bottle around ship" method, and Eu^{3+} was further modified on C-dots@MIL-53 by post-synthesis. Under 308 nm UV light, the as-synthesized Eu^{3+}/C-dots@MIL-53 composites showed two emissions from C-dots and Eu^{3+}. With the increasing addition of TDA, the emission intensity of Eu^{3+} at 616 nm was decreased, while no obvious change was observed in the emission intensity of CD. The ratio of intensities ($I_{c\text{-}dots}/I_{Eu}$) showed a linear relationship with the TDA concentration change, and demonstrated high sensitivity with LOD of 6.8 μg/mL and high selectivity even in simulated urine sample. Luminescence lifetime of Eu^{3+}/C-dots@MIL-53 showed a proportional decrease with the continuous addition of TDA, indicating that the non-radiative deactivation was enhanced by the collision of Eu^{3+}/C-dots@MIL-53 and TDA through the vibrations of TDA(N-H), thus quenching the fluorescence.

Glutathione (GSH) is crucial in many biological processes, such as gene regulation and metabolism. Jalili *et al.* fabricated a dual-emissive ratiometric sensor (BYCDs@ZIF-8) by simultaneously embedding CDs (YCDs) with yellow light emitting and CDs (BCDs) with blue light emitting in ZIF-8 [97]. BYCDs@ZIF-8 maintained the crystal structure as well as the morphology of ZIF-8, and exhibited two fluorescence emissions respectively originated from BCDs ($E_m = 440$ nm) and YCDs ($E_m = 565$ nm) under 365 nm UV irradiation. With the addition of Cu^{2+} to BYCDs@ZIF-8 suspension, Cu^{2+} would interact with the amino groups of YCDs and form a new complex, inhibiting the photoinduced electron transfer (PET) and enhancing the emission intensity of YCDs. The new complex showed a new absorption peak in UV-vis spectra, and the intensity could be enhanced with the concentration increase of Cu^{2+}. Moreover, the new absorption band of Cu^{2+}-YCDs complex overlapped the fluorescence spectrum of BCDs, which transferred the fluorescence resonance energy from BCDs to the complex formed by Cu^{2+} ions and the residual of *O*-phenylenediamine (*O*-PD) ligands of YCDs, thus quenching the fluorescence of BCDs. With the addition of GSH in the system of BYCDs@ZIF-8-Cu^{2+}, Cu^{2+} was reduced to Cu^{+}. Thus, the complex formed by Cu^{2+} and YCDs was disrupted, and the emission intensities of both YCDs and BCDs were recovered. A linear relation can be constructed with the quenching efficiency $[(F_{565}/F_{440})_0/(F_{565}/F_{440})]$ and the concentration of GSH, in which the LOD was calculated as 0.9 nmol/L, demonstrating the ratiometric sensing toward GSH.

4.1.5. Environmental factors

In this sector, the "environmental factors" mainly include moisture/water, pH and temperature. Since the presence of water can make certain organic reactions dangerous or limit their efficiency, and can be detrimental to the storage of food, medicine, *etc.*, the

moisture content must be strictly controlled or even not allowed in some production processes or special environments. Dong *et al.* fabricated a dual emission Eu-MOF/N,S-CD composites (precursors of the Eu-MOF: $Eu(NO_3)_3{\cdot}6H_2O$, 1,3,5-benzenetricarboxylic acid), which were used as a colorimetric sensor for sensing water in organic solvents [53]. The blue emission of N,S-CDs (420 nm) would be restricted due to the aggregation and the confinement of N,S-CDs in Eu-MOFs in organic solvents. While, the red emission of Eu-MOFs (623 nm) would be quenched by the effect of O-H oscillators in water. With the increasing addition of water in Eu-MOF/N,S-CD ethanol suspension, the blue emission intensity was enhanced, and the red emission was quenched under 365 nm UV light. The intensity ratio I_{420}/I_{623} showed a linear increase with the increasing water content in the water contents ranging from 0.05% to 4% with LOD being 0.03%.

Wu *et al.* encapsulated p-CDs (CDs with *p*-phenylenediamine as a precursor) into a MOF which was prepared with indium (In) and 2,2′-bipyridine-5,5-dicarboxylic acid (H_2bpydc), and finally obtained a two-emission hybrid (Tb^{3+}@p-CDs/MOF) with post modification of Tb^{3+} [98]. Different from N,S-CDs in Wu's work [53], under UV irradiation, p-CDs could aggregate in water to display a weak red-light emission. The finely dispersed p-CDs in ethanol, dimethylformamide (DMF) and cyclopropane could display strong red-light emission signal. Thus, Tb^{3+}@p-CDs/MOF was adopted to detect the water molecules in organic solvents as a ratiometric and colorimetric fluorescent sensor. With the increasing addition of water, red light emission at 605 nm quenched and green light emission of Tb^{3+} at 545 nm appeared. The intensity ratio of I_{545}/I_{605} showed a linear relation with the water content, and LOD in ethanol, DMF and cyclopropane were calculated as 0.28%, 0.33% and 0.25% respectively. Moreover, Tb^{3+}@p-CDs/MOF could also be applied in sensing the relative humidity in environment with high sensitivity.

Temperature and pH are also crucial factors in environment, scientific research and industry. CDs@UiO-66-$(OH)_2$ [58], which was mentioned in heavy metal cations section and used as a Fe^{3+} sensor, was also sensitive to temperature and pH. With the temperature increase from 25 °C to 110 °C, the fluorescence intensity at 464 nm showed a linear decrease. Moreover, the fluorescence intensity can be switched more than five cycles between the temperature at 30 and 95 °C. Owing to the protonation-deprotonation of the functional groups on the surface of CDs@UiO-66$(OH)_2$ under different pH, the fluorescence intensity decreased linearly with pH increasing from 3.0 to 7.0. Based on the above, CDs@UiO-66-$(OH)_2$ showed great potential in detecting temperature and pH as a multi-functional sensor.

CNDs@ZIF-8-3, fabricated by calcinating ZIF-8 for 3 h, exhibited two temperature-sensitive fluorescence emission peaks under 380 nm UV-light [59]. Because of the thermal activation of nonradiative decays and relaxation, both intensities of those two emission peaks decreased linearly with the temperature increasing from 278 K to 473 K. Feng *et al.* prepared C-QDs@UiO-66-$(COOH)_2$ by physically mixing C-QDs and UiO-66-$(COOH)_2$ and further fabricated C-QDs@UiO-66-$(COOH)_2$ composite film by electrophoretic deposition [99]. Similar to CNDs@ZIF-8-3 [59], thermal activation of nonradiative decays and relaxation made the fluorescence decrease with the temperature increasing from 97 K to 297 K. A linear relationship between temperature and fluorescence intensity was found and the relative sensitivity reached 1.3% K^{-1} at 297 K.

4.2. Electrochemical sensors

Considering the electrically insulating nature of most MOFs materials, some conducting materials like graphene and carbon blocks have been used to assemble with MOFs for improving the electrical conductivity [38]. Recently, some researchers tried to assemble CDs with MOFs to enhance the electrochemical sensing performance (Table 4).

By integrating graphene quantum dots (GQDs) with a mesoporous porphyrinic zirconium-based MOF (PCN-222), a hybrid material (GQD-PCN-22) was designed and further deposited on fluorine-doped tin oxide (FTO) conductive glass substrates as an electrochemical sensing film [45]. Due to the charge transfer from GQDs as electron-donor to the electron-withdrawing porphyrinic linkers, the conductivity of GQD-PCN-22 was higher than those of PCN-222 and GQDs. Further, the amperometric sensing tests with GQD-PCN-22 film in determination of nitrite oxidation were carried out. Results in Fig. 8a showed that the current density of GQD-PCN-22 was increased with the increasing addition of nitrite. LOD of 6.4 μmol/L was obtained in the range of 40-18000 μmol/L, which showed higher sensitivity than those of GQDs and PCN-22. In this work, electrochemical performance could be enhanced with the assembly of GQDs in MOFs by realizing the donor-acceptor charge transfer.

Gu *et al.* prepared an Apt/CDs@ZrHf-MOF/AE aptasensor for the sensitive and selective sensing of human epidermal growth factor receptor-2 (HER2) and living HER2-overexpressed MCF-7 cells [100]. The Apt/CDs@ZrHf-MOF/AE aptasensor was constructed by dropping CDs@ZrHf-MOF (CDs modified with a bimetallic ZrHf MOF (ZrHf-MOF)) suspension on to the pre-treated Au electrode (AE) surface and further anchored the aptamer by incubating it in HER2 aptamer solution. The incorporation of CDs could improve the electrochemical activity and provide a small electron-transfer resistance (R_{ct}) value of CDs@ZrHf-MOF/AE. Apt/CDs@ZrHf-MOF/AE aptasensor could recognize HER2 by forming G-quadruplex between aptamer strands and HER2. The result showed that the R_{ct} values increased with the increase of HER2 concentration in the range of 0.1 pg/mL to 5 ng/mL (Fig. 8b). LOD of the Apt/CDs@ZrHf-MOF/AE aptasensor for HER2 sensing was measured with electron impedance spectroscopy (EIS) and differential pulse voltammetry (DPV) method, which were calculated as 30 fg/mL and 19 fg/mL, respectively. This electrochemical platform was applied in sensing HER2 ions in human serum samples. Recoveries of HER2 ions in real samples were found in the range of 95.7%-108.3%. Similarly, the electrochemical platform was used for sensing living MCF-7 cells which can release the HER2 marker, and a low LOD with 23 cells/mL was obtained with cyclic voltammetry (CV) method. In addition, this Apt/CDs@ZrHf-MOF/AE aptasensor showed outstanding selectivity, stability, reproducibility, as well as acceptable applicability for sensing both HER2 and MCF-7 cells.

A molecularly imprinted electrochemical sensor (MIP/Au@Cu-MOF/N-GQDs/GCE) for patulin was reported [101]. N-GQDs were firstly decorated on glassy carbon electrodes (GCEs), and then coated with Au@Cu-MOF. The membrane of MIP was grown on Au@CuMOF/N-GQDs/GCE with electropolymerization by cyclic voltammetry (CV) to modify the sensor. The Au@Cu-MOF/N-GQDs/GCE showed a strong peak at −0.11V in PBS due to the transformation of Cu(II) into Cu(I) and Cu, which decreased after MIP combined with electron transfer blocking, increased after the template removal with electron transfer channels forming, and decreased with the presence of patulin. DPV was measured to explore the possibility of the modified sensor (MIP/Au@Cu-MOF/N-GQDs/GCE) for patulin sensing. With the increase of patulin concentration, the response peak of MIP/Au@Cu-MOF/N-GQDs/GCE was decreased (Fig. 8c), which demonstrated a linear relationship in the range of 0.001-70.0 ng/mL (Fig. 8d). Based on quantitative analysis, LOD of 0.0007 ng/mL was obtained. The synergistic effects of N-GQDs and Au@Cu-MOF enabled a larger scale and more sensitive detection range than that of MIP/Au@Cu-MOF/GCE (Figs. 8c and d). In addition, this sensor was successfully applied in patulin sensing in apple juice, and recoveries in these real samples were more than 97%.

Table 4
QD-MOF composites based electrochemical sensors for sensing.

Type of modified Electrode	Synthesis method	Electrochemical technique	Analytes	LOD	Linear range	Real samples	Ref.
GQD-PCN-222	Physical mixing (impregnation method)	Amperometric	Nitrite	6.4 μmol/L	40-18000 μmol/L	-	[45]
CDs@ZrHf-MOF	Bottle around ship	EIS	HER2	30 fg/mL	0.0001–10 ng/mL	Human serum samples	[100]
		DPV		19 fg/mL	0.0001–10 ng/mL		
		CV	Living MCF-7 cells	23 cells/mL	100-10^5 cells/mL		
MIP/Au@Cu-MOF/N-GQDs/GCE	-	DPV	Patulin	0.0007 ng/mL	0.001-70.0 ng/mL	Apple juice	[101]
MOF@CCQDs/NiF	Electrodeposition	CV	D-Tyr	6.12×10^{-6} mol/L	0.2-1.2 mmol/L	-	[61]

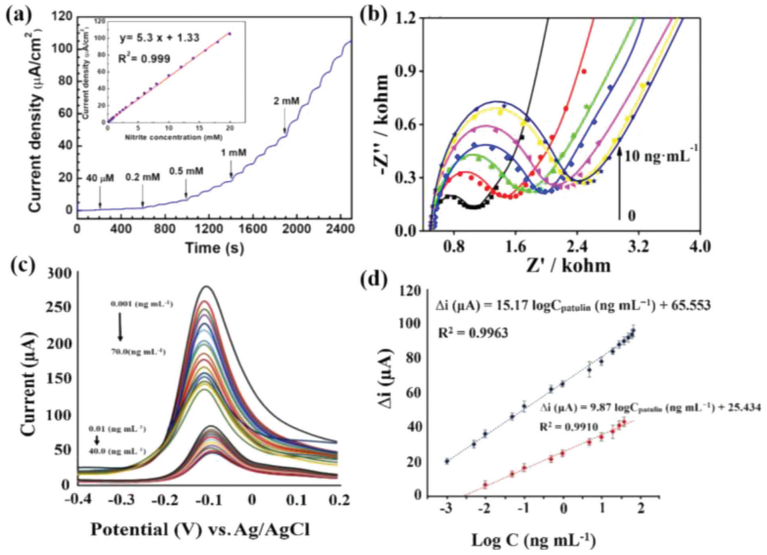

Fig. 8. (a) Current *J*–*t* diagram of GQD-PCN-222 with nitrite in 0.1 mol/L NaCl aqueous solution (Applied potential being +0.9 V). Inset: diagram of current density and nitrite concentration. Copied with permission [45]. Copyright 2019, American Chemical Society. (b) Charge-transfer resistance (R_{ct}) values with HER2 sensing. Copied with permission [100]. Copyright 2019, Elsevier. (c) DPV determination of MIP/Au@Cu-MOF/N-GQDs/GCE and MIP/Au@Cu-MOF/GCE in phosphate buffer solution (0.1 mol/L, pH 7.0) containing patulin with different concentrations. (d) The linear relationships of the current difference (Δi) and logarithm concentration of patulin for the MIP/Au@Cu-MOF/N-GQDs/GCE (blue line) and MIP/Au@Cu-MOF/GCE (red line). (c, d) Copied with permission [101]. Copyright 2020, Elsevier.

Another CD-MOF composite, MOF@CCQDs/NiF, was fabricated for electrochemical sensing tyrosine (Tyr) isomers including L-Tyr and D-Tyr [61]. The modification procedure was carried out with a simple one-pot electrodeposition method by casting CCQDs and Cu-TDPAT MOF on the nickel foil. Due to the highly interconnected network structure of MOF and the exposure of more chiral sites on the porous skeleton surface, the composite electrode exhibits excellent electrochemical behaviors with increased current signals peak for L-Tyr and D-Tyr. The current showed a linear relationship with L-Tyr and D-Tyr concentrations in the range of 0.2-1.2 mmol/L. The LOD of the proposed method for L-Tyr and D-Tyr was obtained 6.12×10^{-6} mol/L and 9.85×10^{-7} mol/L, respectively. Moreover, the modified electrode showed satisfactory stability, reproducibility and excellent selectivity performance.

4.3. Other application

Apart from the applications in photocatalytic and sensing, other applications of CD-MOF also capture researchers' attention, such as electrocatalysis [102], drug delivery [103,104], fluorescence imaging [103], light-emitting diodes [105] and optical anti-counterfeiting [106].

An electrocatalyst for highly oxygen evolution reaction (OER) was fabricated by introducing CDs in a Ni-based MOF with "bottle around ship" method [102]. The obtained electrocatalyst (CDs@MOF) presents comparable onset *i.e.* 1.50V *vs.* RHE (reversible hydrogen electrode) and overpotential *i.e.* 1.55 V (320 mV) *vs.* RHE with other electrocatalysts based on MOF. Low values of the Tafel slope (62 mV/dec) and charge-transfer resistance (R_{ct}, 4.335 Ω) were obtained after the incorporation of CDs into MOFs, speeding the shift of electron and greatly enhancing the conductivity of CDs@MOF composites. High electrochemical active surface area (ECSA, 216.6 cm^2) of CDs@MOF provided enormous active sites for OER. The turnover frequency (TOF) of CDs@MOF was 1.8 s^{-1}, higher than those of the individual MOF (0.007 s^{-1}) and CDs (0.000049 s^{-1}), further demonstrating the potential of CDs@MOF as an electrocatalyst.

In He's work, the green light emitting C-dots@ZIF-8 with external porosity was successfully exploited with "bottle around ship" method for cell imaging and anticancer drug delivery [103]. 5-fluorouracil (5-FU) was chosen and loaded in C-dots@ZIF-8 with no

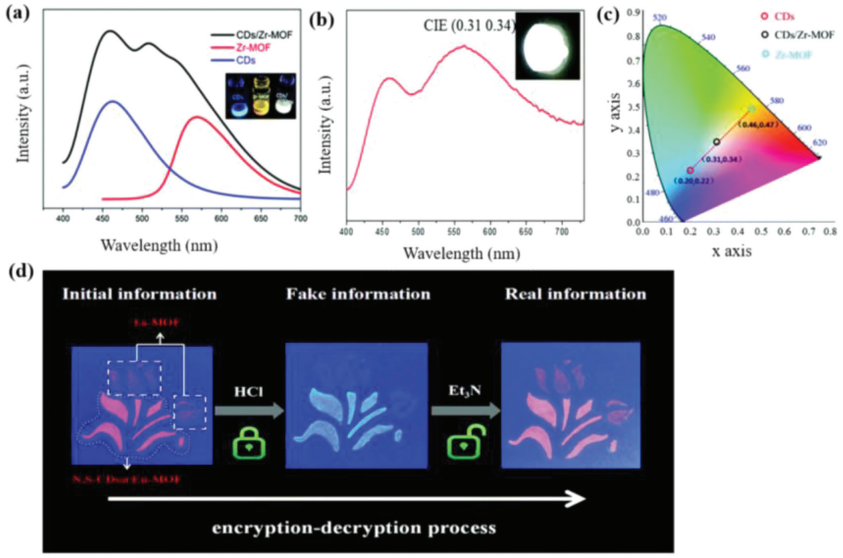

Fig. 9. (a) Emission spectra of CDs, Zr-MOF and CDs/Zr-MOF ($\lambda_{ex} = 365$ nm). (b) Emission spectrum of WLED of the CDs/Zr-MOF composite deposited on a 365 nm InGaN LED chip. Inset picture is the WLED. (c) CIE color coordinates of CD LEDs (0.20, 0.22), Zr-MOF LEDs (0.46, 0.47) and CDs/Zr-MOF WLEDs (0.31, 0.34). (a-c) Copied with permission [105]. Copyright 2019, the Royal Society of Chemistry. (d) Reversible fluorescence images of Eu-MOF and N,S-CDs@Eu-MOF as inks in encryption and decryption process. Copied with permission [106]. Copyright 2020, the Royal Society of Chemistry.

destruction of the C-dots@ZIF-8 structure. Remarkably, 5-FU loaded C-dots@ZIF-8 could release 5-FU more efficiently in acidic PBS solution (92%) than that in neutral PBS solution (67%), which acted as a carrier for pH-responsive drug release in tumor cells with favorable biocompatibility. The author demonstrated that 5-FU loaded C-dots@ZIF-8 with green fluorescence could be successfully applied in cell imaging by endocytosis entering into Hela cells.

To eliminate the use of rare earth (RE) ions in Light-emitting diodes (LEDs), researchers made great efforts to exploring other phosphors materials. Among their studies, MOF-based composites demonstrated great possibility in RE-free LED applications [107–109]. Wang *et al.* synthesized CDs/Zr-MOF composites with binding agent ([3-(2-aminoethylamino)propyl]tri-methoxysilane (AEATMS)) linked for white LEDs (WLEDs) application [105]. The emission of Zr-MOF changed from orange to bright yellow with the presence of AEATMS. After introducing the blue emissive CDs, the CDs/Zr-MOF composites exhibited three broad emissions under 365 nm excitation (Fig. 9a), which attributed to CDs and Zr-MOF respectively. Researchers demonstrated WLED application by optimizing the white light emitting properties with adjusting the fabrication parameters and depositing the composites onto the commercial InGaN LED chips available at 365 nm. The emission spectra of WLED showed similar emission spectrum with two peaks respectively from CDs (450 nm) and Zr-MOF (565 nm) (Fig. 9b). As demonstrated in the CIE diagram (Fig. 9c), the LED tones could be adjusted from yellow, warm white to blue, which corresponded to three chromaticity coordinates of (0.46, 0.47) (Zr-MOF LEDs), (0.31, 0.34) (CDs/Zr-MOF WLEDs) and (0.20, 0.22) (CDs LEDs). Notably, no obvious degradation was found with CDs/Zr-MOF after 3 months of exposure to air, implying that it was potentially stable, nontoxic phosphor solid-state lighting material.

Double-emission materials with self-calibration property and less environmental interference have attracted wide attention as safety information ink in optical anti-counterfeiting. Gao *et al.* reported an Eu based MOF (Eu-MOF) ($Eu_3(OH)(1,3\text{-}db)_2(H_2O)_4]\cdot 3H_2O$ (1,3-db = 1,3-di(3′,5′-dicarboxylpheny)benzene)) and a N,S-CDs@Eu-MOF as two fluorescent high security inks for reversible on/off switching luminescent signal for confidential information in encryption and decryption [106]. Remarkably, the red emission of Eu-MOF could be quenched in hydrogen chloride vapor and reappeared under Et_3N vapor. With the contact of water molecules, N,S-CDs could emit blue emission, and the fluorescence of Eu^{3+} was quenched by the vibration of the O-H bonds. While in organic solvents, red emission of Eu^{3+} recovered and the fluorescence of CDs was quenched because of the agglomeration. Thus, N,S-CDs@Eu-MOF possessed solvent-dependent photoluminescence, which performed N,S-CD related blue luminescence in water as well as Eu-MOF related red emission in organic solvents. Based on these results, Eu-MOF and N,S-CDs@Eu-MOF were dispersed in DMF to prepare two security inks to spray the patterns with a special pen and template, which sprayed Eu-MOF ink as “flowers” and N,S-CDs@Eu-MOF ink as “leaves” (Fig. 9d). Both the flowers and leaves were almost invisible under natural light but emitted red light under UV light. In the encryption process, the flowers disappeared and leaves turned blue under the HCl vapor. Under Et_3N steam, the red flowers reappear, thus realizing the decryption process.

5. Conclusion and perspective

As summarized in this review, versatile MOFs have been used to combine with CDs to fabricate CD-MOF composites with unique properties. By exploiting the inherent properties of CD-MOF composites, enhanced performance in photocatalytic, sensing, electrochemical and other applications can be realized. This review has systematically summarized recent studies on the synthetic methods, characteristics and applications of CD-MOF composites.

In the synthesis of CD-MOF composites, CD precursors and pre-synthesized MOF or MOF precursors and pre-synthesized CD are usually needed. Two popular methods are “ship in a bottle” and “bottle around the ship”, which can encapsulate CDs in the MOF matrix. “Physical mixing” tends to immobilize CDs on the surface of MOF. “*In situ* encapsulated” method construct CD-MOF composites with simple operation and less solvent. Besides, other emerging methods to fabricate CD-MOF composites have been reported. These employed methods display special advantages for different application, but most of them consume lots of organic solvents and are inefficient in controlling the shape, size and composition of CD-

MOF composites. Thus, future research will focus on the CD-MOF composites preparation technique with rational design, easy operation, environmental protection and low cost.

Applications discussed in this review benefit from the rationally combination of the CDs with exceptional photophysical and photochemical properties and MOFs with high surface area and massive porosity. The unique advantages of MOF in the field of catalysis, sensing and other applications were already well-known. The introduced CDs can serve as multiple roles in different CD-MOF composites, like electron receptor, photosensitizer and/or spectral converter in photocatalytic systems, fluorescence signal supporter in fluorescence sensing, and high conductive materials in electrochemical application. Obvious advantages of CD-MOF composites in the field of photocatalysis are reducing charge recombination and improving the utilization of solar energy. In the sensing field, CD-MOF composites with dual-emission or multi-emission can improve the accuracy in quantification and anti-interference ability. Some CD-MOF composites can also improve the electronic conductivity to enhance the electrochemical sensing and electrocatalytic performance. More efforts are still needed to accomplish wide application of CD-MOF composites in practical production.

(1) Constructing 0D/2D CD-MOF composites for photocatalysis and electrochemical applications. As the low dimension is beneficial for the space separation of light-excited charge carriers and the enhancement of charge transfer [110,111], the combination of zero-dimensional CDs and two-dimensional MOFs is a feasible way to fabricate catalysts with excellent performance. Moreover, the electrical conductivity of 0D/2D CD-MOF composites can be improved, due to the formation of planar π–d conjugated sheet of MOF with 2D structure [112].
(2) Controlling the position of CDs precisely on MOFs. As can be seen from the above analysis, the position of CD on MOF has great influence on the properties of CD-MOF composites. For example, the generation of CD in MOF pores can form rich heterojunctions, which is conducive to the separation of photogenerated electrons and holes, thus improving the photocatalytic performance. Therefore, “ship in a bottle” and “bottle around ship” can be more suitable for CD-MOF composites-based catalysts construction. The construction of core–shell structure or egg yolk structure of CD-MOF composites with “physical mixing” method can provide more surface area, which is beneficial for sensing. Besides the selection of synthesis method, the control of the location of functional groups attached to the organic linkers of MOF and the modification of CD surface with specific ligand are helpful for the precise control of CDs position in CD-MOF composites.
(3) Improving the selectivity of CD-MOF composites-based sensors. Rationally design of the pore size and functional sites of the MOF, as well as the size of CDs are helpful for realizing the selective target detection.
(4) Strengthening the researches concerning the fluorescence sensing mechanism. Sensing mechanisms like competitive adsorption, photoelectron transfer (PET), resonant energy transfer (FRET) and intermolecular charge transfer (ICT) are usually determined and analyzed with experimental tests such as XRD, UV-vis spectra and fluorescence lifetime analysis. The combination of experiment investigations with theoretical calculations is helpful for the deep understanding of the relationship between the structure and property, host-guest interaction, and synergistic effects, thus accelerating the development of CD-MOF composites.
(5) Boosting the stability of CD-MOF composites. The photo stability and the stability of CD-MOF composites in different environments, especially under strong alkaline and acidic conditions, still needs to be considered for applications in multiple cycles.
(6) Fabricating workable devices. Most of the CD-MOF composites demonstrations were conducted using laboratory-prepared samples, and applied in powder form which is averse to recovery and separation. To achieve recyclability and overcome the difficulty in the separation of CD-MOF composite, CD-MOF composites can be grown on some substrate with film form and fabricated to integrated devices, which is closer to practical applications.
(7) Extending the application of CD-MOF composites. The applications of CD-MOF are concentrated in the fields of photocatalysis and fluorescence sensing, and more researches need to be done in the fields of electrochemical sensing, electrocatalysis and anti-counterfeiting, which display great application prospects. As to the environmental remediation applications, most of the CD-MOF composites were used as photocatalysts for Cr(VI), organic dyes and aromatic compounds degradation. More organic pollutants should be selected to examine the photocatalytic efficiencies of CD-MOFs.
(8) Reducing the fabrication cost. The cost of synthetic process and precursor materials have limited the extensive practical application of CD-MOF composites. Therefore, the development of sustainable methods or utilization of low cost raw materials were crucial tasks for the researchers to realize the practical applications of CD-MOF composites.

Despite many challenges, it was believed that more profound understanding on CD-MOF composites in synthesis and application will be achieved. In the future, those researches will present growing amount of information to guide researchers in rationally designing CD-MOF composites and enabling their large-scale application.

Declaration of competing interest

The authors declare that they have no known competing financial interests or personal relationships that could have appeared to influence the work reported in this paper.

Acknowledgments

This work was supported by the Natural Science Foundation of Jiangsu Province (No. BK20210856), the Science and Technology Project of Changzhou City (No. CJ20210117) and the Industry-Academic Cooperation Project of Jiangsu Province (No. BY2021278).

References

[1] A. Corma, H. García, F.X. Llabrés i Xamena, et al., Chem. Rev. 110 (2010) 4606–4655.
[2] J. Liu, L. Chen, H. Cui, et al., Chem. Soc. Rev. 43 (2014) 6011–6061.
[3] Q. Zhao, X.H. Yi, C.C. Wang, et al., Chem. Eng. J. 429 (2021) 132497.
[4] T. Xia, Y. Lin, W. Li, et al., Chin. Chem. Lett. 32 (2021) 2975–2984.
[5] S. Li, F. Wu, R. Lin, et al., Chem. Eng. J. 429 (2022) 132217.
[6] X.D. Du, S. Wang, F. Ye, et al., Environ. Res. 206 (2022) 112414–112429.
[7] G. Si, X. Kong, T. He, et al., Chin. Chem. Lett. 32 (2020) 918–922.
[8] C. Ji, Y. Ren, H. Yu, et al., Chem. Eng. J. 430 (2022) 132960.
[9] J. Mayans, M. Winterlich, D. Mchugh, et al., Dalton Trans. 50 (2021) 6997–7006.
[10] S. Singh, S. Kaushal, J. Kaur, et al., Chemosphere 272 (2021) 129648.
[11] J.R. Li, J. Sculley, H.C. Zhou, Chem. Rev. 112 (2012) 869–932.
[12] T. Yıldız, I. Erucar, Chem. Eng. J. 431 (2022) 134263.
[13] S. Chen, X. Li, J. Duan, et al., Chem. Eng. J. 419 (2021) 129653.
[14] Y. He, W. Zhou, G. Qian, et al., Chem. Soc. Rev. 43 (2014) 5657–5678.
[15] L.J. Murray, M. Dincă, J.R. Long, Chem. Soc. Rev. 38 (2009) 1294–1314.
[16] J. Zheng, X. Cui, Q. Yang, et al., Chem. Eng. J. 354 (2018) 1075–1082.
[17] T. Rasheed, F. Nabeel, Coord. Chem. Rev. 401 (2019) 213065.
[18] L. Chen, D. Liu, J. Peng, et al., Coord. Chem. Rev. 404 (2020) 213113.
[19] Y.Q. Zhang, S.S. Sheng, S. Mao, et al., Water Res. 163 (2019) 114883.
[20] Y.Q. Zhang, X.H. Wu, S. Mao, et al., Talanta 204 (2019) 344–352.
[21] Y.Q. Zhang, J.X. Liu, X.H. Wu, et al., Anal. Chim. Acta 1131 (2020) 68–79.
[22] L.H. Wu, S.L. Yao, H. Xu, et al., Chin. Chem. Lett. 33 (2021) 541–546.
[23] T. Simon-Yarza, A. Mielcarek, P. Couvreur, et al., Adv. Mater. 30 (2018) 1707365.

[24] G. Lan, K. Ni, W. Lin, Coord. Chem. Rev. 379 (2019) 65–81.
[25] P. Horcajada, T. Chalati, C. Serre, et al., Nat. Mater. 9 (2010) 172–178.
[26] H.K. Chae, D.Y. Siberio-Pérez, J. Kim, et al., Nature 427 (2004) 523–527.
[27] T. Du, J. Wang, L. Zhang, et al., Chem. Eng. J. 431 (2022) 134050.
[28] P. Goyal, A. Paruthi, D. Menon, et al., Chem. Eng. J. 430 (2022) 133088.
[29] M.S. Yao, W.X. Tang, G.E Wang, et al., Adv. Mater. 28 (2016) 5229–5234.
[30] S.J. Yang, J.Y. Choi, H.K. Chae, et al., Chem. Mater. 21 (2009) 1893–1897.
[31] C.C. Wang, X. Wang, W. Liu, Chem. Eng. J. 319 (2019) 123601.
[32] Y. Shang, Q. Xu, Z. Gao, et al., Chem. Eng. J. 428 (2022) 132536.
[33] T. Wu, X.J. Liu, Y. Liu, et al., Coord. Chem. Rev. 403 (2020) 213097.
[34] X.H. Yan, Y.N. Zhao, G.G. Du, et al., Chem. Eng. J. 433 (2021) 133624.
[35] T. Uemura, N. Yanai, S. Watanabe, et al., Nat. commun. 1 (2010) 83.
[36] J. Lee, O.K. Farha, J. Roberts, et al., Chem. Soc. Rev. 38 (2009) 1450–1459.
[37] J. Lei, R. Qian, P. Ling, et al., TrAC-Trend. Anal. Chem. 58 (2014) 71–78.
[38] S. Kempahanumakkagari, K. Vellingiri, A. Deep, et al., Coord. Chem. Rev. 357 (2018) 105–129.
[39] X. Feng, Y. Ying, Y. Jian, et al., Chem. Eng. J. 303 (2016) 231–237.
[40] Y.P. Sun, B. Zhou, Y. Lin, et al., J. Am. Chem. Soc. 128 (2006) 7756–7757.
[41] S. Zhu, Y. Song, X. Zhao, et al., Nano Res. 8 (2015) 355–381.
[42] B.Z. Li, T.Y. Suo, S.Y. Xie, et al., TrAC-Trend. Anal. Chem. 135 (2021) 116163.
[43] S. Li, K. Ji, M. Zhang, et al., Nanoscale 12 (2020) 9533–9540.
[44] X. Lin, G. Gao, L. Zheng, et al., Anal. Chem. 86 (2014) 1223–1228.
[45] Y.C. Chen, W.H. Chiang, D. Kurniawan, et al., ACS Appl. Mater. Interfaces 11 (2019) 35319–35326.
[46] R. Lin, S. Li, J. Wang, et al., Inorg. Chem. Front. 5 (2018) 3170–3177.
[47] S.G. Khasevani, S. Shahsavari, M.R. Gholami, Mater. Res. Bull. 138 (2021) 111204.
[48] X.B. Meng, J.L. Sheng, H.L. Tang, et al., Appl. Catal. B: Environ. 244 (2019) 340–346.
[49] L. Xu, G. Fang, J. Liu, et al., J. Mater. Chem. A 4 (2016) 15880–15887.
[50] J. Gao, Q. Li, C. Wang, et al., Sens. Actuators B: Chem. 253 (2017) 27–33.
[51] H. Weng, B. Yan, Dalton Trans. 45 (2016) 8795–8801.
[52] X. Fu, R. Lv, J. Su, et al., RSC Adv. 8 (2018) 4766–4772.
[53] Y. Dong, J. Cai, Q. Fang, et al., Anal. Chem. 88 (2016) 1748–1752.
[54] J.M. Yang, X.W. Hu, Y.X. Liu, et al., Micropor. Mesopor. Mat. 274 (2019) 149–154.
[55] L. Xu, M. Pan, G. Fang, et al., Sens. Actuators B: Chem. 286 (2019) 321–327.
[56] X.Y. Xu, B. Yan, X. Lian, Nanoscale 10 (2018) 13722–13729.
[57] Y. Si, X. Li, G. Yang, et al., J. Mater. Sci. 55 (2020) 13049–13061.
[58] C. Yao, Y. Xu, Z. Xia, J. Mater. Chem. C 6 (2018) 4396–4399.
[59] Y. Wang, B. Wang, H. Shi, et al., Inorg. Chem. Front. 5 (2018) 2739–2745.
[60] B. Li, Z. Zhang, Y. Li, et al., Angew. Chem. Int. Ed. 51 (2012) 1412–1415.
[61] Y. Hou, Z. Liu, L. Tong, et al., Dalton Trans. 49 (2020) 31–34.
[62] C.C. Wang, J.R. Li, X.L. Lv, et al., Energy Environ. Sci. 7 (2014) 2831–2867.
[63] Y.X. Li, X. Wang, C.C. Wang, et al., J. Hazard. Mater. 399 (2020) 123085.
[64] H. Li, C. Zhao, X. Li, et al., J. Alloys Compd. 844 (2020) 156147.
[65] D.D. Chen, X.H. Yi, L. Ling, et al., Appl. Organomet. Chem. 34 (2020) e5795.
[66] X. Wei, P. Wang, H.F. Fu, et al., Mater. Res. Bull. 129 (2020) 110903.
[67] X. Wang, Y.X. Li, X.H. Yi, et al., Chin. J. Catal. 42 (2021) 259–270.
[68] C. Zhao, Z. Wang, X. Li, et al., Chem. Eng. J. 389 (2019) 123431–123446.
[69] W. Xun, L.B. Wen, A. Hf, et al., Environ. Pollut. 249 (2019) 502–511.
[70] X.H. Yi, F.X. Wang, X.D. Du, et al., Appl. Organomet. Chem. 33 (2019) e4621.
[71] R. Wang, K.Q. Lu, Z.R. Tang, et al., J. Mater. Chem. A 5 (2017) 3717–3734.
[72] X.T. Qin, T.T. Qiang, L. Chen, et al., Micropor. Mesopor. Mat. 315 (2021) 110889.
[73] Q. Wang, G. Wang, X. Liang, et al., Appl. Surf. Sci. 467-468 (2019) 320–327.
[74] S. Safa, M. Khajeh, A.R. Oveisi, et al., Adv. Powder Technol. 32 (2021) 1081–1087.
[75] S. Safa, M. Khajeh, A.R. Oveisi, et al., Chem. Phys. Lett. 762 (2021) 138129.
[76] Y.Z. Zhang, Y.R. Dai, L.F. Yin, et al., Catal. Sci. Technol. 10 (2020) 3654–3663.
[77] C.X. Duan, L.L. Xie, S.Y. Wang, et al., Chemosphere 291 (2022) 132873.
[78] C. Zheng, X. Qiu, J. Han, et al., ACS Appl. Mater. Interfaces 11 (2019) 42243–42249.
[79] D. Wei, W. Tang, Y. Gan, et al., Catal. Sci. Technol. 10 (2020) 5666–5676.
[80] J.M. Yang, X.W. Hu, Y.X. Liu, et al., Micropor. Mesopor. Mat. 274 (2018) 149–154.
[81] R. Lin, F. Li, S. Liu, et al., Angew. Chem. 125 (2013) 13671–13675.
[82] Z. Dou, J. Yu, Y. Cui, et al., J. Am. Chem. Soc. 136 (2014) 5527–5530.
[83] X. Zhang, Q. Hu, T. Xia, et al., ACS Appl. Mater. Interfaces 8 (2016) 32259–32265.
[84] X. Zhang, Q. Zhang, D. Yue, et al., Small 14 (2018) 1801563.
[85] J. He, J. Xu, J. Yin, et al., Sci. China Mater. 62 (2019) 1655–1678.
[86] J. Hao, F. Liu, N. Liu, et al., Sens. Actuators B: Chem. 245 (2017) 641–647.
[87] X.Y. Xu, B. Yan, J. Mater. Chem. C 4 (2016) 1543–1549.
[88] M.R. Razanajatovo, W.Y. Gao, Y.R. Song, et al., Chin. Chem. Lett. 32 (2021) 2637–2647.
[89] Z. Wu, H. Yang, S. Pan, et al., ACS Sens. 5 (2020) 2211–2220.
[90] Y. Wang, J. He, M. Zheng, et al., Talanta 191 (2019) 519–525.
[91] P. Azimi, D. Zhao, C. Pouzet, et al., Environ. Sci. Technol. 50 (2016) 1260–1268.
[92] R. Wu, S. Xie, Environ. Sci. Technol. 51 (2017) 2574–2583.
[93] S.B. Kim, H.T. Hwang, S.C. Hong, Chemosphere 48 (2002) 437–444.
[94] J.S. Li, Y.J. Tang, S.L. Li, et al., CrystEngComm 17 (2015) 1080–1085.
[95] Y. Zou, F. Yan, T. Zheng, et al., Talanta 135 (2015) 145–148.
[96] S.J. Qin, B. Yan, Sens. Actuators B: Chem. 272 (2018) 510–517.
[97] R. Jalili, A. Khataee, M.R. Rashidi, et al., Sens. Actuators B: Chem. 297 (2019) 126775.
[98] J.X. Wu, B. Yan, Dalton Trans. 46 (2017) 7098–7105.
[99] J.F. Feng, S.Y. Gao, J. Shi, et al., Inorg. Chem. 57 (2018) 2447–2454.
[100] C. Gu, C. Guo, Z. Li, et al., Biosens. Bioelectron. 134 (2019) 8–15.
[101] B. Hatamluyi, M. Rezayi, H.R. Beheshti, et al., Sens. Actuators B: Chem. 318 (2020) 128219.
[102] M.Y.U. Rehman, S. Manzoor, N. Nazar, et al., J. Alloys Compd. 856 (2021) 158038.
[103] L. He, T. Wang, J. An, et al., CrystEngComm 16 (2014) 3259–3263.
[104] Q. Jia, Z. Li, C. Guo, et al., Nanoscale 11 (2019) 20956–20967.
[105] A. Wang, Y.L. Hou, F. Kang, et al., J. Mater. Chem. C 7 (2019) 2207–2211.
[106] J.P. Gao, R.X. Yao, X.H. Chen, et al., Dalton Trans. 50 (2020) 1690–1696.
[107] H. Cai, L.L. Xu, H.Y. Lai, et al., Chem. Commun. 53 (2017) 7917–7920.
[108] Q. Li, J. Luo, L. Wang, et al., CrystEngComm 19 (2017) 214–217.
[109] T. Mondal, S. Mondal, S. Bose, et al., J. Mater. Chem. C 6 (2018) 614–621.
[110] Q. Liu, T. Chen, Y. Guo, et al., Appl. Catal. B: Environ. 193 (2016) 248–258.
[111] D.Q. Zeng, T. Zhou, W.J. Ong, et al., ACS Appl. Mater. Interfaces 11 (2019) 5651–5660.
[112] X. Huang, P. Sheng, Z. Tu, et al., Nat. Commun. 6 (2015) 7408.